The enigma of the Albian Gap: spatial variability and the competition between salt expulsion and extension

Leonardo M. Pichel* and Christopher A-L. Jackson

Basins Research Group (BRG), Department of Earth Science and Engineering, Imperial College London, South Kensington Campus, SW7 2BP, United Kingdom

Abstract

The Albian Gap is a uniquely large (up to 65 km wide and >450 km long), enigmatic salt-related structure in the Santos Basin, offshore Brazil. It is located near the basin margin and trends NE (i.e. sub-parallel to the Brazilian coastline). The gap is characterized by a near-complete absence of Albian strata above depleted Aptian salt. Its most remarkable feature is an equivalently large, equally as enigmatic, seaward-dipping, supra-salt rollover that contains a post-Albian sedimentary succession that is up to 9 km thick. Due to its unique geometry, size, and counter-regional aspect, the origin and evolution of the Albian Gap has been the centre of debate for >25 years. This debate revolves around two competing models; i.e. did it form due to thin-skinned (i.e. supra-salt) extension, or progradational loading and salt expulsion? The extension-driven model states that the Albian Gap (and overlying rollover) formed due to post-Albian gravity-driven extension accommodated by slip on a large, counter-regional, listric normal fault (the Cabo Frio Fault). Conversely, the expulsion-driven hypothesis states that the Albian Gap was established earlier, during the Albian, and that post-Albian deformation was controlled by differential loading, vertical subsidence, and basinward salt expulsion in the absence of significant lateral extension. This study utilizes a large (c. 76,000 km^2), dense (4-8 km line spacing), depth-migrated, 2D seismic dataset that fully covers and which thus permits, for the first time, a detailed, quasi-3D structural analysis of the entire Albian Gap. In this study we focus on: i) the evolution of base-salt relief and the original salt thickness variations; and ii) the geometry of the post-Albian rollover, and its related faults and salt structures. To constrain the kinematics of the Albian Gap, and how this relates to the evolution of the base-salt relief, we also apply novel structural restoration workflows that incorporate flexural isostasy, in addition to a detailed, sequential reconstruction of the intra-gap rollover sequences. Our results show that the geometry and kinematics of the Albian Gap vary along-strike, and that both post-Albian extension *and* expulsion

play a significant role in its evolution. Seaward-dipping growth wedges, salt rollers, and listric normal faults record extension, whereas sigmoidal wedges, halokinetic sequences, and upturned near-diapir flaps, the latter two associated with large diapirs bounding the downdip edge of the gap, record basinward salt expulsion and inflation. Where the Albian gap is relatively wide (>50 km), these processes alternate and operate at approximately equal proportions. Our results are consistent with the amount of basinward translation inferred from the analysis of ramp-syncline basins located downdip on the São Paulo Plateau. Our results seemingly reconcile one of the longest-running debates in salt tectonics, as well as having more general implications for understanding the regional kinematics and dynamics of salt-related structures in other salt basins, in particular the controls on the development of large, counter-regional faults.

1. Introduction

Salt-bearing passive margins are typified by kinematically-linked domains of updip extension, midslope translation, and downdip contraction and/or salt advance (e.g. Rowan et al., 2004; Peel 2014; Jackson et al., 2015; Jackson and Hudec, 2017). Each of these domains are associated with a complex and variable suite of salt structures. Updip areas of extension are characterized by reactive diapirs, salt rollers, and salt-detached, listric normal faults, whereas downdip areas of contraction are dominated by salt-cored (buckle) folds, thrusts, and actively rising, squeezed diapirs. Intermediate translational domains can have both styles of deformation when developed above variable base-salt relief (Brun and Fort, 2011; Jackson et al., 2015; Dooley et al., 2016; 2018; Pichel et al., 2019b,c). One of the largest and perhaps the most controversial salt structures is the Albian Gap in the Santos Basin, Brazil. It trends NE, is up to 65 km wide in its south-central part, and extends sub-parallel to the Brazilian margin for nearly the entire length of the Santos Basin (c. 450 km long). The gap is located at the boundary between the extensional and translational domains, and is characterized by the near-complete absence of Albian strata and an equally large, up to 55 km wide, Late Cretaceous-Paleogene counter-regional (i.e. basinward-dipping) rollover that overlies depleted Aptian salt (Fig. 1) (Demercian et al., 1993; Mohriak et al., 1995; Davison et al., 2012; Guerra and Underhill., 2012; Fiduk and Rowan, 2012; Quirk et al., 2012; Jackson et al., 2015).

Due to its unique size, geometry and counter-regional aspect, the Albian Gap has been the centre of debate for >25 years (Fig. 2). This debate revolves primarily around its origin and evolution, which have been variably described by either an *extension-* (Fig. 2a) and *expulsion-driven model* (Fig. 2b). Many authors propose an extension-driven origin in which the rollover and the gap itself formed due to post-Albian gravity-

driven extension associated with slip on a large, counter-regional, salt-detached normal fault, the Cabo Frio Fault (CFF, fig. 1), which accommodates 30-55 km of lateral displacement (i.e. heave; Fig. 2a) (Cobbold and Szatmari, 1991; Demercian et al., 1993; Mohriak et al., 1995; Davison et al., 2012; Guerra and Underhill., 2012; Rowan and Ratcliff, 2012; Quirk et al., 2012). Others suggest an expulsion-driven origin in which the gap was established earlier, during the Albian and post-Albian, with deformation driven by differential loading, vertical subsidence, and basinward expulsion of salt generating a post-Albian expulsion rollover. This model does not require or invoke significant lateral extension or overburden translation (Szatmari et al., 1996; Ge et al., 1997; Gemmer et al., 2005; Krezcek et al 2007; Adam and Krézsek, 2010; Jackson et al., 2015). Cross-section based restorations of the Albian Gap have not yet resolved this debate, as the gap can be reasonably restored either by post-Albian extension (Fig. 2a), or basinward salt expulsion following Albian diapirism (Fig. 2b) (Rowan and Ratliff, 2012; Jackson et al., 2015). In the former model (Fig. 2a), the post-Albian rollover is equivalent to the hangingwall of a counter-regional, salt-detached normal fault, with diapirs and minibasins in its footwall translating basinward for a distance equal to the fault heave. In the latter model (Fig. 2b), the rollover is restored by basinward salt expulsion from a diapir that decreases in width through time, and in which there is no lateral movement of basinward minibasins and associated salt structures.

These two competing hypotheses are intrinsically related to another long-lived controversy, the general salt tectonics and structural evolution of the São Paulo Plateau, a large, basement-cored structural high located immediately downdip of the Albian Gap (Fig. 2b). In the extension-driven model, post-Albian extension within the Albian Gap is kinematically balanced by the lateral movement of salt and overburden

51 contraction on the São Paulo Plateau (Guerra and Underhill, 2012; Fiduk and Rowan,
52 2012; Quirk et al., 2012; Rowan and Ratliff, 2012). Conversely, in the expulsion-driven
53 model, post-Albian deformation is characterized by salt inflation and intense, intra-salt
54 deformation, but *not* significant overburden translation and contraction (Ge et al.,
55 1997; Gemmer et al., 2004; Jackson et al., 2015a,b).

56 Solving these debates is crucial to our understanding of the regional kinematics and
57 dynamics of salt-bearing passive margins and, thus, their geodynamic evolution (cf.
58 Jackson et al., 2015). Selecting the appropriate kinematic model will help us
59 geometrically balance basin-scale deformation, and constrain the timing, style, and
60 magnitude of salt movement, deformation, and sub-horizontal translation, the latter
61 typically being problematic due to cryptic diapir shortening and extension (Hossack et
62 al., 1995; Rowan and Ratliff., 2012; Jackson et al., 2015a). Understanding when and
63 how salt and its overburden deforms has important implications for hydrocarbon
64 exploration along salt-bearing margins, given it can help us constrain the location and
65 timing of hydrocarbon migration and trap formation, and the timing of deposition of key
66 petroleum system elements (e.g. source, reservoir, and seal rocks; Jackson et al.,
67 2015; Allen et al., 2016; Pichel et al., 2018).

68 We present, for the first time, a detailed geometric and kinematic analysis of the Albian
69 Gap. Whereas most previous studies focused on only 1 or 2, dip-orientated (i.e. NW-
70 trending) cross sections through the centre of the gap where it is widest (Demercian
71 et al., 1993; Mohriak et al., 1995; Ge et al., 1997; Fiduk and Rowan, 2012; Guerra and
72 Underhill, 2012; Jackson et al., 2015), we analyse several dip- and strike-oriented
73 sections to understand its true 3D geometrical and possibly kinematic variability. We
74 use an extensive and modern, 2D depth-migrated seismic dataset. Small 2D line
75 spacing (4-8 km) provides a dense, quasi-3D grid with which to analyse lateral and

vertical variations in base-salt relief, salt and growth strata geometries, and overburden faulting within the Albian Gap. In addition, we restore three cross-sections from different parts of the Albian Gap, focusing on the overlying post-Albian rollover, bounding salt structures, and detachment geometry. By doing this, we are able to constrain the contribution of different mechanisms (i.e. extension and expulsion) to the formation of the gap and, we hope, solve one of the longest-lived controversies in salt tectonics.

2. Geological Setting

The Santos Basin covers c. 3.5×10^5 km^2 and is bound by the Cabo Frio High to the northeast and by the Florianopolis Platform to the southwest (Mohriak et al., 1995; Garcia et al., 2012). The basin originated as a rift during the Early Cretaceous in response to the opening of the South Atlantic (e.g., Meisling et al., 2001; Modica and Brush, 2004; Karner and Gambôa, 2007; Mohriak et al., 2008). Grabens and half-grabens were oriented predominantly NNE-NE due to ESE-SE directed extension and were filled by largely Barremian, fluvial-lacustrine deposits that are overlain by an early-to-middle Aptian, carbonate-dominated succession (Meisling et al., 2001; Davison et al., 2012). The number of active faults and their rate of slip decreased during the Aptian and, by the Late-Aptian, a c. 2.5-4 km thick salt succession was deposited (De Freitas, 2006; Davison et al., 2012; Garcia et al., 2012). Salt deposition was controlled by an inherited rift topography, resulting in marked spatial variations in original salt thickness (Davison et al., 2012; Garcia et al., 2012; Rodriguez et al. 2018). In sub-salt lows such as the Merluza Graben (Fig. 1b) (cf. Mohriak et al., 2010), salt was up to c. 4 km thick (Garcia et al., 2012; Lebit et al., 2019). Conversely, on sub-salt highs such as the Outer High (Fig. 1b), salt was only c. 1.5-2 km thick (Garcia et al., 2012; Rodriguez et al., 2018).

During the early Albian, the Santos Basin experienced fully marine conditions due to thermally induced, post-rift subsidence and a rise in eustatic sea-level. This resulted in widespread deposition of a carbonate-dominated succession that was up to c. 1 km thick updip and which thinned basinward to c. 200 m on the São Paulo Plateau (Fig. 1b) (Modica & Brush, 2004). During the late Albian, the basin tilted south-eastward, inducing gravity gliding of the salt and its overburden. Salt-related deformation produced numerous thin-skinned, predominantly basinward-dipping, salt-detached normal faults that dismembered the Albian carbonate platform into rafts in the updip extensional domain (zone of extension, fig. 1) (Demercian et al., 1993; Cobbold et al., 1995; Guerra and Underhill, 2012; Quirk et al., 2012). The Albian Gap, the focus of our study, is located at the basinward (i.e. south-eastern) edge of the extensional domain (Fig. 1).

Post-Albian sedimentation was characterized by margin-scale clastic progradation, with sediments derived from the uplifting of the Serra do Mar mountain range (Fig. 1a) (Modica & Brush, 2004). Most late Albian faults in the updip extension domain became inactive by the end of the Albian and deformation migrated downdip into the Albian Gap and onto the São Paulo Plateau (SPP) (Fig. 1) (Quirk et al., 2012; Jackson et al. 2015a). Post-Albian salt tectonics was characterized by basinward salt evacuation from the Albian Gap, local salt welding (Davison et al., 2012; Jackson et al., 2014; 2015a), and up to c. 30 km of overburden translation further downdip in the São Paulo Plateau (Pichel et al., 2018; 2019c). The base-salt relief and salt thickness variations associated with the inherited rift topography impacted salt tectonics on the São Paulo Plateau, generating flow partition with localized contraction, extension and passive diapirism (Garcia et al., 2012; Pichel et al., 2018; 2019c).

3.1 Dataset and Methods

3.1. Seismic Data and Interpretation

We use a vast (c. 76,000 km^2 areal coverage), zero-phased processed, Kirchoff pre-stack depth-migrated 2D seismic dataset covering nearly the entire length of the Santos Basin and the Albian Gap (Fig. 1). The 2D survey comprises NW- and NE-trending profiles that are oriented sub-parallel to the dip- and strike-direction of the basin (and Albian Gap), respectively (Fig. 1c). Given the size of the Albian Gap, the seismic dataset has a relatively small line spacing (c. 4 km and 8 km between dip- and strike-orientated profiles, respectively), giving it a quasi-3D character. Seismic profiles have a total record length of 16 km and we display images following the Society of Economic Geologists (SEG) normal polarity convention, whereby a downward increase in acoustic impedance is represented by a positive reflection event (white on greyscale seismic sections) and a decrease in acoustic impedance by a negative event (black on greyscale seismic section) (Brown, 2011). The seismic data almost fully images the updip extensional domain and partly images the intermediate translational and minibasin province (cf. Pichel et al., 2018; 2019; Lebit et al 2019), intersecting the updip portion of the 3D seismic dataset used by Jackson et al. (2015b) and Pichel et al. (2018; 2019) (Fig. 1).

We mapped base- and top-salt based on their distinct seismic expression and overburden geometries (Fig. 3). As we did not have direct access to borehole data, mapping of key post-salt horizons were based on their tectono- and seismic-stratigraphic significance, with age-calibration provided by a number of recently published, borehole-constrained cross-sections (Garcia et al., 2012; Guerra and Underhill., 2012; Quirk et al., 2012; Hadler-Jacobsen et al., 2014; Jackson et al., 2015a; Rodriguez et al., 2018). We mapped an Top Albian unconformity (blue) to

outline the geometry and extent of the Albian Gap (Fig. 4), and a prominent Paleogene regional unconformity (yellow) that marks the end of bulk salt deformation across most of the basin (cf. Fiduk and Rowan, 2012; Garcia et al., 2012; Guerra and Underhill, 2012; Jackson et al., 2015b). We also mapped key post-Albian (Upper Cretaceous-Paleocene) horizons within the Albian Gap rollover to constrain its present structural style and to infer its evolution via isopach (thickness map) analysis.

3.2. Restorations

To restore geometries imaged on seismic reflection profiles we combine decompaction and unfolding by simple vertical shear, and move-on-fault algorithms, following established restoration workflows for salt-related deformation (cf. Rowan and Ratliff 2012). Instead of restoring only a single profile (Ge et al., 1997; Rowan and Ratliff, 2012; Guerra and Underhill, 2012; Jackson et al., 2015), we perform 2D structural restorations of three of the most representative profiles from the Albian Gap. We restore these profiles to a gently-dipping, clinoform-like seabed that is characteristic of many prograding clastic slopes (cf. Hadler-Jacobsen et al. 2014); by doing this, we incorporate geologically more realistic geometries not applied in previous restorations of the Albian Gap. Although commonly gentle (c. 1°), the foresets of margin-scale prograding clinoforms can reach up to 16° (Patruno et al., 2015), dipping 0.5-2° and being c. 50-300m tall in the study-area (see present-day seabed, figs. 6-10). Thus, previous workflows that restored post-Albian rollover horizons to a flat top (cf. Rowan and Ratliff, 2012; Jackson et al., 2015) have likely distorted their original geometries, as well as the gap itself. We reconstruct the approximate paleo-seabed through time using the present seabed as template and local erosional unconformities and toplaps as additional constraints. Although estimating the paleobathymetry over time involves some uncertainty, clear stratal terminations in and around the Albian Gap afford

confidence in our workflow and, we argue, allows a more accurate representation of growth strata geometries than previous achieved.

We also incorporate flexural isostatic compensation in our restorations; we apply this immediately after sequential decompaction of the stratigraphic succession. This allows us to quantify and remove the effects of differential loading and basin subsidence, and to provide more accurate estimates of the base-salt geometry, regional dip, and related salt thickness through time. This ultimately permits us to establish the key boundary conditions governing the evolution of the Albian Gap. The decompaction is performed using the Sclater and Christie (1980) function and assumes a carbonate (Albian) and siliciclastic (post-Albian) overburden; this is in agreement with borehole-constrained studies in the area (Guerra and Underhill, 2012; Hadler-Jacobsen, 2014). For the flexural isostasy, we use a crustal density of 2.78 g/cm^3 and lithospheric elastic thickness (T_e) of 5 km. We also test T_e values of 1.5, 10 and 15 km but choose T_e = 5 km as we (and others; Scotchman et al., 2006; 2010) argue this is a more valid approximation for highly-stretched continental crust; the same value has been applied by other studies focused on the geodynamic evolution of the Santos Basin (Garcia et al., 2012; Rodriguez et al., 2019). We perform a detailed sequential restoration of the central and most representative section within the Albian Gap involving 12 steps from Aptian (top-salt) to present. We then restore additional sections back to the Albian and Aptian; this allows us to constrain spatial variations in the original dimension of the Albian Gap and the original Aptian salt thickness, and the overall basin geometry and depth.

4. Albian Gap Structural Framework

The Albian Gap is c. 450 km long. It varies in width from 10-15 km in the northeast (North Santos Basin) to 30-50 km in its central portion, widening to 65 km in its central-

south portion, before narrowing again to 15 km to the southwest (Figs. 4, 6-12). The gap is widest (c. 50-65 km) updip of the Sugar-Loaf and Tupi Sub-Highs (cf. Rodriguez et al., 2018; Pichel et al. 2019), and where it is intersected by a large NNE-SSW-striking basement-involved fault (i.e. the Merluza Fault, Mohriak et al., 2011) in the southwest (Figs. 3 and 4). The gap is associated with a post-Albian, basinward-dipping rollover that is of equivalent length, 6-10 km thick, and up to 55 km wide. This rollover overlies salt that is strongly depleted or apparently welded salt (Figs. 5a and 6-12). The salt layer ranges from nearly welded in places (<50 m thick) to an average of 100 m thick and up to 500 m thick salt rollers (Figs 5b and 6-8).

4.1. Salt and Fault Geometries

Counter to that previously described, the Albian Gap is not defined on its basinward edge by a single, through-going (i.e. c. 450 km long), landward-dipping listric fault (Cabo Frio Fault, cf. Mohriak et al., 1995; Guerra and Underhill, 2012; Fiduk and Rowan, 2012; Quirk et al., 2012). It is instead bound by a series of smaller (4-12 km long) fault segments and associated salt rollers (Figs. 6-11). Salt rollers occur within or defining the outboard margin of the Albian Gap (R in figs. 6-11). The ones within the gap are relatively small (200-500 m tall on average) (Figs. 6-8), although some are up to 1.2 km tall (Fig. 12). Rollers bounding the seaward side of the gap are larger (1-1.5 km tall) than those within the gap *but* occur only in the northern and southern sectors of the structure (Figs. 10-11). These rollers are broadly asymmetric and triangular in shape, and are commonly defined on their landward sides by landward-dipping listric normal faults (Figs. 6-9), although basinward-dipping faults also occur in the north (Fig. 10) and south of the gap (Fig. 11). In some cases, both sides of the salt rollers are flanked by different-age packages of wedge-shaped strata that towards them. Such geometries have been described by Quirk and Pilcher (2012), who argue

they document a temporal switch in fault polarity from one diapir flank to the other (Figs. 10-11) (so-called “flip-flop salt tectonics”; Quirk and Pilcher., 2012).

The dominant landward-dipping faults contain 0.4-1 km thick, basinward-thickening wedges in their hangingwall. Equivalent-age strata are thin or absent on their footwalls (Figs 6-7). Where strata are missing, we estimate fault heaves of c. 2-6 km using the width of their hangingwall growth wedges. Salt rollers and faults generally become younger, larger, and display greater displacement basinward as indicated by their progressively younger growth strata and their shallower tip heights (Figs. 6-9). This indicates that extension migrated basinward.

The basinward limit of the Albian Gap is, therefore, commonly defined by a partially-to-fully fault-bounded diapir (Figs. 6-7). Where the gap is relatively narrow (<30 km), the diapir is asymmetric and triangular in cross-section, a geometry characteristic of reactive (i.e. extensional) diapirs and/or salt rollers (cf. Vendeville and Jackson, 1992; Jackson and Hudec, 2017) (Figs. 9-10). However, in the central portion of the gap, where it is relatively wide (>30 km) (Fig. 6-8 and 11), the geometry and size of the bounding diapir are markedly different and *cannot* be entirely explained by post-Albian extension. In this location the diapirs are irregular and semi-circular in plan-view, rather than linear like those seen to the north and south where extension dominates (Figs. 3 and 5). The diapirs are 8-12 km wide, up to 4 km tall, and are *partially* defined by a landward-dipping listric fault on their landward margins (Figs. 6-7). Locally upturned and thinned strata are also observed near the tops of the diapirs on their landward margins. In contrast, their basinward margins are *always* flanked by locally upturned and thinned strata (Figs. 6-7). In other cases, the diapirs are narrower (2-4 km wide), taller (>4.5 km) and have upturned and thinned strata on both of its flanks with no evidence of extension (Fig. 8). This upturned strata can vary from km-scale,

so-called composite halokinetic sequences (i.e. CHSs) (cf. Giles and Rowan 2012; Pichel and Jackson 2020) or multi-km upturned flaps (cf. 'megaflaps' of Rowan et al. 2016). Larger flaps are more common on the basinward flanks of the gap-bounding diapirs, whereas CHSs typically occur on their landward sides, within the Albian Gap. Both cases indicate that the diapirs bounding the central and widest portion of the Albian Gap were largely influenced (Figs. 6-7) and, in places (Fig. 8), driven by a combination of passive and active salt rise after an initial phase of reactive rise. Active and especially active rise are load-driven processes and, thus, can occur in the absence of extension (Rowan et al., 2003; Jackson and Hudec, 2017). This suggests that both post-Albian differential loading and extension occurred within the Albian Gap.

4.2. Rollover Geometries

In addition to the intra- and gap-bounding diapirs, the post-Albian rollover geometries also vary in terms of their geometry and origin (Figs. 6-8). They can be characterized by i) basinward-thickening wedges that expand towards landward-dipping, salt-detached (listric) normal faults (Figs. 6-9); or ii) sigmoidal wedges that are thicker in their centre, but which thin and downlap basinward towards the salt, onto 'stranded', intra-gap Albian blocks or the footwalls of salt rollers (Figs. 6-8).

Whereas the first geometry is readily linked to regional gravity-driven extension (Fig. 13a) (cf. Brun and Mauduit, 1997; Rowan et al., 1999; Jackson and Hudec, 2017), the second cannot be explained by the same process. Besides, similar sigmoidal, basinward-dipping and -thinning wedges occur landward of the Albian Gap where they clearly downlap the Albian interval (Fig. 7); this geometry cannot be readily explained by slip on a normal fault or, therefore, record extension. We interpret that these sigmoidal geometries are associated with prograding clinoforms that were later rotated

by the deflation and basinward expulsion of salt (Fig. 13b) (cf. Ge et al., 1997; Jackson and Hudec, 2017). They occur predominantly in the central-south portion of the Albian gap where it is widest (>35 km, figs. 6-8). We make the key observations that the wider the gap, the more abundant are the sigmoidal wedges, and the larger is the seaward-bounding diapir (Figs. 6-7).

The Albian Gap lies downdip of the Serra do Mar mountain range (Fig. 1), which formed during the Late Cretaceous-Eocene, coeval with the formation of the Albian Gap rollover (Mohriak et al., 1995; Guerra and Underhill, 2012). Continental uplift resulted in erosion and basinward progradation clastic sediments into the Albian Gap (Modica and Brush, 2004; Guerra and Underhill., 2012). Where the gap is wider and prograding sigmoidal geometries abound, the post-Albian margin prograded further seaward (Fig. 14). Where the gap is relatively narrow (<35 km), basinward-thickening wedges dominate, indicating that, in these areas, the gap appeared to have formed primarily in response to extension (Figs. 9-10). In summary, we show a positive relationship between the amount of post-Albian shelf-margin progradation, the amount of salt expulsion and thinning, and overall gap width.

4.3. Base-salt Structure and Polarity

Throughout most of the Albian Gap, the base of the salt presently dips gently (<1.5°) landward and salt-detached extension is controlled by landward-dipping normal faults that are antithetic to the overall basinward direction of gravity-driven transport (Figs. 6-9). At its south and north portions, however, this changes. In its northern portion where it narrows abruptly to <14 km, the gap is bound by a flip-flop roller and a basinward-dipping normal fault (Fig. 10). In its southernmost portion, basinward of a major pre-salt rift structure, the Merluza Graben, the Albian Gap is bound on its seaward side by basinward-dipping, salt-detached normal faults (Fig. 11). The Merluza

Fault has a throw of 3.5 km at the base-salt and is associated with the largest diapir (c. 8.5 km tall and 10 km wide) within the study-area (and possibly the entire basin, Fig. 3b). This suggests that the graben was a major structural low prior to and during (and possibly after) salt deposition, resulting in initially locally thickened salt (c. 2.5-4 km thick). Other small, landward-dipping, basement-involved sub-salt faults produced 0.5-1 km of structural relief at the base-salt and, thus, contribute to a regionally rugose base-salt beneath the Albian Gap (Figs. 3a and 6-9).

The thicker succession of Aptian salt within the Merluza Graben resulted in: i) partition of salt flow with increased diapiric rise updip of the Albian Gap and, ii) a locally steeper, basinward-dipping base-salt within the Albian Gap due to tilting of the footwall of the Merluza Fault. The large (c. 10 km wide) diapir near the south-eastern edge of the Merluza Graben produced an additional c. 10 km of separation of the Albian interval given the diapir was growing *during* the Albian (i.e. Albian strata were not deposited above it). Further basinward, the steeper basinward-dipping base-salt influenced the style of salt-detached faulting here, which is predominantly synthetic (i.e. basinward-dipping) and in marked contrast to other areas of the Albian Gap.

5. Restoration

5.1. Kinematics on a salt-detached slope

Previous structural restorations of the Albian Gap were ambiguous, meaning that the Albian Gap could be restored by purely salt expulsion and vertical subsidence (expulsion-model), *or* regional extension (extension-model) (Rowan and Ratliff, 2012; Jackson et al. 2015). This ambiguity is at least partly due to the fact these restorations: i) have not incorporated the variable rollover stratal geometries (i.e. sigmoidal clinoforms associated with margin progradation vs. basinward-thickening wedges

associated with fault slip), ii) incrementally restored the rollover succession to a flat-top, distorting the original (i.e. syn-depositional) stratal geometries, iii) have not included the effects of flexural isostasy, keeping the base-salt static through time, iv) did not incorporate kinematic constraints provided by structural geometries seen immediately downdip on the São Paulo Plateau. Here we present for the first time, a detailed sequential restoration of the Albian Gap incorporating these aspects (Fig. 15).

In the main restored section (Fig. 7), the Albian Gap is presently c. 50 km wide. The cumulative heave on faults flanked by basinward-thickening, fault slip-related wedges documents c. 26 km of post-Albian extension (Fig. 15a-l). This is equivalent to c. 50% of the current width of the gap, demonstrating that by Albian times the gap was already there in the form of a c. 24 km wide, c. 2.8 km tall, and 90-100 km long reactive/passive diapir (Fig. 15m). Early post-Albian sequences (g, h, j and l) were primarily associated with basinward progradation of the basin margin by clinoform accretion (Figs. 6-8), and vertical subsidence due to salt thinning and lateral expulsion. Overlying sequences were predominantly affected by sub-horizontal extension of the overburden (a-f and i; Fig. 15). Additional restored sections in the central portion of the Albian Gap show that post-Albian extension varied from 26-28 km ($\pm$ 2 km) (Figs. 15 and 16). All restorations show that where it is presently widest, the gap was already partly formed during the Albian in the form of a 24-30 km wide passive diapir (Figs. 14 and 15); this reactive diapir was initially narrower (<2 km) where the gap is presently narrower (<30 km, fig. 16). Our restorations show that the variable *present width* of the Albian Gap was primarily controlled by the *original width* of the gap during the Albian (i.e. Albian diapir). They also show that post-Albian extension in the central portion of the Albian Gap (figs. 6-9) showed little along-strike variability (24-28 km, according to our restorations; Figs 15-17). Extension nonetheless varied laterally

throughout the full length of the Albian Gap, being as little as 10-12 km in the northernmost portion where the gap is presently narrower (Fig. 10).

The measurements of extension have a small margin of error (5-10%), but nonetheless agree with estimates of 28-32 km of post-Albian translation of salt and overburden obtained from the analysis of ramp-syncline basins downdip on the São Paulo Plateau (Pichel et al., 2018). We argue that area was kinematically linked to the Albian Gap, being equivalent to its (mega)footwall.

5.2. Loading and Flexural Isostasy

Flexural isostasy is associated with the long-wavelength effects driven by the isostatic response of the crust to sediment loading (e.g. Roberts et al., 1998; Scotchman et al., 2008; Garcia et al., 2012). Flexural isostasy assumes that any load on the lithosphere is supported by flexural bending stresses within the immediate area surrounding the load. Applying flexural isostasy to structural restorations has been shown to yield the most geologically realistic results in backstripping workflows (Roberts et al., 1998; Scotchman et al., 2008). In the Santos Basin, the base-salt beneath and near the Albian Gap presently dips 0.5-1.5° landward for at least 150 km in the dip direction (Figs. 6-10), with the exception being the more strongly basinward-dipping footwall of the Merluza Fault in the south (section 4.3, fig. 11). This is anomalous when compared to the majority of passive margin salt basins such as in Campos and Espirito Santo basins, offshore Brazil (Mohriak et al., 2012; Davison et al., 2012; Dooley et al. 2016), West and Northwest Africa (Marton et al., 2000; Tari et al., 2003; 2012; Hudec and Jackson, 2004; Peel 2014; Pichel et al., 2019), and the Gulf of Mexico (Rowan et al., 2004; Hudec et al., 2018), where the detachment presently dips regionally basinward.

Our restorations show that this somewhat unusual, landward-dipping attitude of the salt detachment in the Santos Basin relates to the presence of the equally enigmatic and large (450 km long, up to 55 km wide and 10 km thick), post-Albian rollover associated with the Albian Gap (fig. 6). The restorations also demonstrate that the base-salt originally dipped basinward 1.2-1.5° (on average) and that it switched polarity progressively through time due to proximal loading by the thick, post-Albian sequence now overlying and filling the Albian Gap (Figs. 14-16). The landward dip of the base-salt was, nonetheless, established relatively early, during deposition of the two lowermost post-Albian sequences (Fig. 14). Deposition and thus isostatic loading were focused within the Albian Gap as salt was being expelled from underneath it. Salt expulsion and diapir growth basinward of the gap generated a barrier that hindered the basinward transport of sediment (cf. Modica and Brush, 2004; Hadler-Jacobsen, 2014).

Our restorations also show that the original salt thickness was 0.8-1.2 km over pre-salt highs, 1-2 km in the Albian Gap, and 1.4-2.8 km further downdip and over pre-salt lows (Figs. 14-16). Although involving a degree of uncertainty due to, for example, the out-of-plane movement of salt (cf. Rowan and Ratliff, 2012), our top-salt restorations are based on, we argue, valid assumptions that the salt was in depositional connection across pre-salt highs and that unfolding to a gently (<0.5°) basinward-dipping regional datum is permissible (see Hudec and Norton, 2019; Hudec et al., 2019). Our measured depositional salt thicknesses are consistent with the estimates of Davison et al. (2012), Garcia et al. (2012), and Rodriguez et al. (2018).

6. Discussion

6.1. Albian Gap kinematics: expulsion vs. extension

6.1.1. Evidence of Extension

In this study we identified three geometries evidence for gravity-driven, salt-detached, post-Albian extension within the Albian Gap. These are: i) salt rollers, ii) listric normal faults; iii) basinward-thickening wedges. Moreover, ramp-syncline basins that indicate 28-32 km of salt-detached basinward translation on the São Paulo Plateau downdip of the Albian Gap (cf. Pichel et al., 2018) are another diagnostic of equivalent gravity-driven extension within the Albian Gap as seen from the restorations (Figs. 15-17).

6.1.2. Evidence of Expulsion

Despite the aforementioned evidence for extension, the sum of observed heaves (<30 km) on individual salt-detached normal faults and stratal separations associated with related diapirs (i.e. rollers) cannot account for the entire separation of the Albian interval where the gap is >30 km wide (Figs. 6-8). Moreover, contrasting diapir and related growth strata geometries suggest an additional control on its evolution. Three additional observations suggest that post-Albian basinward salt expulsion also played a role in the formation of the Albian Gap: i) basinward-thinning sigmoidal wedges that downlap onto deflated salt and/or remnant (i.e. intra-gap) Albian blocks; ii) bounding active diapirism; and iii) halokinetic sequences or upturned flaps. These are all driven by vertical subsidence and differential loading, completely independent of extension. Moreover, previous quantitative analysis of the Albian Gap rollover (cf. Ge et al., 1997; Jackson et al., 2015a) shows an asymmetric dip-depth relationship for growth strata bounding the gap-bounding diapirs, also arguing against a purely extensional origin.

6.2. Albian Gap Model

We have argued that the Albian Gap was formed by a combination of thin-skinned extension and salt expulsion (i.e. differential loading), with these processes operating

in approximately equal proportions where the gap is widest (c. 50-60 km). This is equivalent to c. 25-30 km of post-Albian extension in its central portion, which balances the amount of post-Albian translation recorded in ramp-syncline basins further basinward on the São Paulo Plateau (28-32 km of translation; Pichel et al., 2018). We therefore propose a revised, hybrid model for the Albian Gap in which we combine both processes (Fig. 18).

In our model, the gap was formed by: i) post-Albian salt expulsion due to progradation and differential loading of an Albian salt wall and ii) broadly coeval extension due to basinward translation above an initially basinward-dipping salt detachment (Fig. 18). Post-Albian basinward translation of salt and overburden occurred downdip (footwall) of the Albian Gap, whereas within the gap (hangingwall) only the salt translated basinward. The blocks further landward of the Albian Gap did not move laterally as, by that time, Aptian salt was locally welded and the base-salt had flipped to dip landward due to isostatic loading by post-Albian clastic sediments (Fig. 18). This model explains why the gap is wider in its south-central portion as a result of greater post-Albian salt mobilization basinward, a process ultimately driven by: 1) greater local salt supply related to the presence of an initially volumetrically larger, Albian salt wall, and 2) greater basinward progradation of post-Albian clastic sediments.

Our model is analogous to the 'heel-keel model' (cf. Krézsek et al., 2007; Jackson and Hudec, 2017) where there is a switch from early basinward-dipping faulting to later landward-dipping fault. In our case, during the Albian, extension was accommodated primarily by basinward-dipping listric faults (Fig. 18b). Continuous sedimentary loading in their hangingwalls drove salt withdrawal, increasing basal drag and ultimately stopping the associated thin-skinned deformation (cf. Krezsek et al., 2007). Salt expulsion from their hangingwalls resulted in salt inflation and, consequently, a large

445 diapir formed further downdip; this diapir acted as topographic high above which no
446 Albian sediments were deposited (Fig. 18b). This area was, consequently, able to
447 move faster than the updip depleted salt segment. This resulted in additional 24-30
448 km of separation of the Albian interval due to post-Albian progradation above the
449 thicker, more mobile salt and development of counter-regional faults (Fig. 18c-d).

450 These counter-regional faults have thin, tabular successions in their footwalls; in some
451 cases, strata age-equivalent to that observed in their hangingwalls are locally absent,
452 meaning that their footwall is mostly formed by younger hangingwall growth strata of
453 a basinward fault (Figs. 6-8). This suggests that these faults formed over inflated salt
454 lacking pre-extension Albian sediments and that their footwall was primarily composed
455 of salt expelled from beneath their adjacent hangingwalls (Fig.18b-c). In other words,
456 the Albian was not deposited uniformly within the study-area and that, by the beginning
457 of the Late Cretaceous, the Albian Gap was already partially present in the form of a
458 20-30 km wide passive diapir (Fig. 18; see also restorations in Fig. 15-17). This initial
459 diapiric gap could be explained by a combination of reactive and passive salt rise
460 during the Albian (see Jackson et al., 2015). The additional 25-30 km of separation of
461 the Albian interval was subsequently accommodated by post-Albian extension. This
462 resulted in the basinward expulsion of salt from within this Albian diapir onto the São
463 Paulo Plateau, where salt inflation and 28-32 km of translation are observed (Figs. 15-
464 18) (c.f. Jackson et al., 2015; Pichel et al., 2019c).

465 **6.3. Why the predominance of counter-regional faults?**

466 In gravity-driven systems, downdip salt flow over a basinward-dipping detachment
467 typically results in the extension being preferentially accommodated by synthetic (i.e.
468 basinward-dipping) normal faults (Brun and Fort, 2011; Quirk et al., 2012; Jackson
469 and Hudec, 2017). Why was post-Albian extension along most of the extensional

domain in the Santos Basin largely accommodated on counter-regional, landward-dipping normal faults? Three possible hypotheses may explain this:

1) Progressive dip reversal of the salt detachment driven by flexural isostasy

2) Inherited base-salt relief associated with pre-salt rift faults

3) Rapid margin-scale progradation above thick salt and salt expulsion basinward

The anomalous counter-regional dip of the salt detachment within the Albian Gap likely influenced the style and polarity of overburden faulting, locally favouring antithetic basal-shear and counter-regional faulting (cf. Brun and Mauduit 2009). However, as seen from our restorations, which explicitly account for flexural isostasy, the detachment originally dipped basinward so that the early development of counter-regional faults and basinward-dipping rollover was not controlled by the detachment dip. The flip in base-salt polarity may, nonetheless, have favoured the development of larger counter-regional faults later in the history of the Albian Gap, after a significantly thick overburden succession was deposited within it (Figs. 6-9).

The several, predominantly landward-dipping base-salt steps associated with earlier-formed rift normal faults produced a rugose base-salt that likely influenced the location and style of supra-salt faulting, as well as local salt rise in the Albian Gap. The nucleation of salt and supra-salt structures by rift-related base-salt topography is demonstrated in several studies (Ge et al., 1997; Adam and Krézsek, 2010; Dooley et al., 2016; 2018; Pichel et a., 2019a,b,c). The base-salt steps within the Albian Gap may have disturbed net-basinward salt flow, favouring the development of listric normal faults and salt rollers with the same polarity to the underlying, base-salt relief that is dominated by landward-dipping steps (Figs. 6-8). However, given that counter-

493 regional faults also appear above areas with a locally flat base-salt (Figs. 7 and 9), this
494 effect appears to be secondary.

495 Physical models of salt-detached rollovers have shown that high-sedimentation rates
496 favour the development of counter-regional (i.e. landward-dipping) faults (Krescek et
497 al., 2007). Prograding margins, such as the Santos Basin, have typically high rates of
498 accommodation generation and sediment input (Modica and Brush, 2004; Hadler-
499 Jacobsen et al., 2014). In the Albian Gap, an anomalously thick (> 9 km) overburden
500 was deposited directly above thick (1.5-2 km) salt during the Late Cretaceous-
501 Paleogene; this was associated with rapid progradation and hinterland uplift in the
502 Serra do Mar (Fig. 1).

503 We propose that the three mechanisms outlined above jointly influenced the geometry
504 and kinematics of the Albian Gap. However, we suspect that the main control on the
505 development of basinward-dipping rollovers and counter-regional faults and,
506 therefore, the key driver for extension within the Albian Gap was differential loading
507 associated with progradation above thick, inflated salt (Figs. 18). This resulted in salt
508 being expelled basinward from beneath prograding clinoforms and from the earlier-
509 formed diapir, up onto the footwall of counter-regional faults (Figs. 15 and 18).

510 **Conclusions**

511 Our study provides the first ever quantification of the contribution between the two
512 competing processes generating the Albian Gap, expulsion vs extension. This is
513 based on systematic analysis of the post-Albian rollover spatial variability and
514 contrasting growth strata geometries, basinward-thickening strata vs sigmoidal
515 clinoform wedges. We identify evidence for post-Albian salt-detached extension as
516 well as evidence for salt expulsion driven by differential loading within the Albian Gap.

This shows that neither pure post-Albian salt expulsion or extension can fully account for the entire separation of the Albian interval, nor the observed rollover and diapir geometries within the Albian Gap. We also provide detailed structural restorations of key sections that, for the first time, combine decompaction, flexural isostasy and unfolding of margin-scale rollover geometries to a gently-dipping seafloor. Moreover, we incorporate the contrasting Albian Gap rollover geometries and measurements of overburden translation from the adjacent São Paulo Plateau as kinematic constraints. We then propose a new model based on the seismic observations and structural restorations that demonstrates that the Albian Gap was formed by a combination of post-Albian extension and salt expulsion at approximately equal proportions where the gap is wider (>50 km). In this model, the gap was already partially established during the Albian as a 20-30 wide salt wall. Additional 25-30 km of extension occurred during the post-Albian driven by margin-scale progradation of sediments over an inflated salt wall, promoting differential loading and salt expulsion basinward onto the São Paulo Plateau. The extension was therefore controlled by differential loading and expulsion of salt basinward, which, coupled with the gradual base-salt dip reversal and presence of base-salt steps favoured the development of counter-regional faults.

Acknowledgements

First, we thank TGS and Western Geco as well as individuals in these companies for granting permission to use seismic data. We also thank Schlumberger for academic licenses of Petrel and Petex for Move. We are also very grateful for discussions with Frank Peel, Olly Duffy, Gillian Apps which significantly helped developing the concepts behind this paper.

References

Allen, H., Jackson, C. A. L., Fraser, A. J. (2016). Gravity-driven deformation of a youthful saline giant: the interplay between gliding and spreading in the Messinian basins of the Eastern Mediterranean. Petroleum Geoscience, 22(4), 340-356.

Brown, A. R. (2011). Interpretation of three-dimensional seismic data. Society of Exploration Geophysicists and American Association of Petroleum Geologists.

Brun, J. P., Fort, X. (2011). Salt tectonics at passive margins: Geology versus models. Marine and Petroleum Geology, 28(6), 1123-1145

Cobbold, P. R., Szatmari, P., Demercian, L. S., Coelho, D., Rossello, E. A. (1995). Seismic and experimental evidence for thin-skinned horizontal shortening by convergent radial gliding on evaporites, deep-water Santos Basin, Brazil, *in*: Jackson, M. P. A., Roberts, D. G., Snelson, S. (eds) Salt tectonics: a global perspective. AAPG Memoir 65, 305-321.

Demercian, S., Szatmari, P., Cobbold, P. R. (1993). Style and pattern of salt diapirs due to thin-skinned gravitational gliding, Campos and Santos basins, offshore Brazil. Tectonophysics, 228(3-4), 393-433.

Davison, I., Anderson, L., Nuttall, P. (2012). Salt deposition, loading and gravity drainage in the Campos and Santos salt basins. Geological Society of London Special Publications, 363(1), 159-174.

Dooley, T. P., Hudec, M. R., Carruthers, D., Jackson, M. P., Luo, G. (2016). The effects of base-salt relief on salt flow and suprasalt deformation patterns—Part 1: Flow across simple steps in the base of salt. Interpretation, 5(1), SD1-SD23.

Dooley, T. P., Hudec, M. R. (2016). The effects of base-salt relief on salt flow and suprasalt deformation patterns—Part 2: Application to the eastern Gulf of Mexico. Interpretation, 5(1), SD25-SD38.

Dooley, T. P., Hudec, M. R., Pichel, L. M., Jackson, M. P. (2018). The impact of base-salt relief on salt flow and suprasalt deformation patterns at the autochthonous, paraautochthonous and allochthonous level: insights from physical models. Geological Society, London, Special Publications, 476, SP476-13.

568 Fiduk, J. C., Rowan, M. G. (2012). Analysis of folding and deformation within layered
569 evaporites in Blocks BM-S-8 &-9, Santos Basin, Brazil. Geological Society, London,
570 Special Publications, 363(1), 471-487.

571 Garcia, S. F., Letouzey, J., Rudkiewicz, J. L., Danderfer Filho, A., & de Lamotte, D. F.
572 (2012). Structural modeling based on sequential restoration of gravitational salt
573 deformation in the Santos Basin (Brazil). Marine and Petroleum Geology, 35(1), 337-
574 353.

575 Ge, H., Jackson, M. P., Vendeville, B. C. (1997). Kinematics and dynamics of salt
576 tectonics driven by progradation. AAPG bulletin, 81(3), 398-423.

577 Gemmer, L., Ings, S.J., Medvedev, S. Beaumont, C. (2004). Salt tectonics driven by
578 differential sediment loading: stability analysis and finite-element experiments. Basin
579 Research, 16(2), 199-218.

580 Giles, K. A., & Rowan, M. G. (2012). Concepts in halokinetic-sequence deformation
581 and stratigraphy. Geological Society, London, Special Publications, 363(1), 7-31.

582 Guerra, M. C., Underhill, J. R. (2012). Role of halokinesis in controlling structural styles
583 and sediment dispersal in the Santos Basin, offshore Brazil. Geological Society,
584 London, Special Publications, 363(1), 175-206.

585 Hadler-Jacobsen, F., Groth, A., Hearn, R.E., and Liestøl, F.M. (2010), Controls on and
586 expressions of submarine fan genesis within a high accommodation margin setting,

587 Santos Basin, Brazil—A high-resolution seismic stratigraphic and geomorphic case
588 study, in Wood, L.J., Simo, T.T., and Rosen, N.C., eds., Seismic Imaging of
589 Depositional and Geomorphic Systems: Gulf Coast Section Society for Sedimentary
590 Geology Foundation Annual Bob F. Perkins Research Conference Proceedings, v. 30,
591 p. 572–615.

592 Hossack, J. (1995). Geometric rules of section balancing for salt structures.

593 Hudec, M. R., Jackson, M. P. A. (2004). Regional restoration across the Kwanza
594 Basin, Angola: Salt tectonics triggered by repeated uplift of a metastable passive
595 margin. AAPG bulletin, 88(7), 971-990.

596 Hudec, M. R., & Norton, I. O. (2019). Upper Jurassic structure and evolution of the
597 Yucatán and Campeche subbasins, southern Gulf of Mexico. AAPG Bulletin, 103(5),
598 1133-1151.

599 Hudec, M. R., Dooley, T. P., Peel, F. J., & Soto, J. I. (2019). Controls on the evolution
600 of passive-margin salt basins: Structure and evolution of the Salina del Bravo region,
601 northeastern Mexico. Geological Society of America Bulletin.

602 Jackson, M.P., Hudec, M.R. (2017). Salt Tectonics: Principles and Practice.
603 Cambridge University Press.

604 Jackson, C. A. L., Jackson, M. P., Hudec, M. R. (2015a). Understanding the
605 kinematics of salt-bearing passive margins: A critical test of competing hypotheses for
606 the origin of the Albian Gap, Santos Basin, offshore Brazil. Geological Society of
607 America Bulletin, 127(11-12), 1730-1751.

608 Jackson, C. A. L., Jackson, M. P., Hudec, M. R., Rodriguez, C. R. (2015b). Enigmatic
609 structures within salt walls of the Santos Basin—Part 1: Geometry and kinematics from
610 3D seismic reflection and well data. Journal of Structural Geology, 75, 135-162.

611 Karner, G. D., Gambôa, L. A. P. (2007). Timing and origin of the South Atlantic pre-
612 salt sag basins and their capping evaporites. Geological Society, London, Special
613 Publications, 285(1), 15-35.

614 Krézsek, C., Adam, J. and Grujic, D (2007). Mechanics of fault and expulsion rollover
615 systems developed on passive margins detached on salt: insights from analogue
616 modelling and optical strain monitoring. Geological Society, London, Special
617 Publications, 292(1), pp.103-121.

618 Lebit, H., Arasanipalai S., Tilton, J. & Ollagnon, P. (2019) Santos Vision: Innovative
619 Seismic Data Processing in a Super Giant Oil Basin. GeoExPro, May, 2019.

620 Marton, G., Tari, G. Lehmann, C (1998). Evolution of salt-related structures and their
621 impact on the post-salt petroleum systems of the Lower Congo Basin, offshore Angola.
622 In: American Association of Petroleum Geologists International Conference and
623 Exhibition, Rio de Janeiro. Extended Abstracts Volume, 834–834.

624 Meisling, K. E., Cobbold, P. R., Mount, V. S. (2001). Segmentation of an obliquely
625 rifted margin, Campos and Santos basins, southeastern Brazil. AAPG bulletin, 85(11),
626 1903-1924.

627 Modica, C. J., Brush, E. R., 2004. Postrift sequence stratigraphy, paleogeography, and
628 fill history of the deep-water Santos Basin, offshore southeast Brazil. AAPG bulletin,
629 88(7), 923-945.

630 Mohriak, W.U., Macedo, J.M., Castellani, R.T., Rangel, H.D., Barros, A.Z.N., Latgé,
631 M.A.L., Mizusaki, A.M.P., Szatmari, P., Demercian, L.S., Rizzo, J.G. Aires, J.R.
632 (1995). Salt tectonics and structural styles in the deep-water province of the Cabo Frio
633 region, Rio de Janeiro, Brazil, *in*: Jackson, M. P. A., Roberts, D. G., Snelson, S. (eds)
634 Salt tectonics: a global perspective. AAPG Memoir 65, 273-304.

635 Mohriak, W., Nemčok, M., Enciso, G. (2008). South Atlantic divergent margin
636 evolution: rift-border uplift and salt tectonics in the basins of SE Brazil. Geological
637 Society, London, Special Publications, 294(1), 365-398.

638 Mohriak, W. U., Nóbrega, M., Odegard, M. E., Gomes, B. S., & Dickson, W. G. (2010).
639 Geological and geophysical interpretation of the Rio Grande Rise, south-eastern
640 Brazilian margin: extensional tectonics and rifting of continental and oceanic crusts.

641 Mohriak, W. U., Szatmari, P., Anjos, S. (2012). Salt: geology and tectonics of selected
642 Brazilian basins in their global context. Geological Society, London, Special
643 Publications, 363(1), 131-158.

644 Patruno, S., Hampson, G. J., & Jackson, C. A. (2015). Quantitative characterisation of
645 deltaic and subaqueous clinoforms. Earth-Science Reviews, 142, 79-119.

646 Peel, F. J. (2014). The engines of gravity-driven movement on passive margins:
647 Quantifying the relative contribution of spreading vs. gravity sliding mechanisms.
648 Tectonophysics, 633, 126-142.

649 Pichel, L. M., Peel, F., Jackson, C.A.-L., Huuse, M., 2018, Geometry and kinematics
650 of salt-detached ramp syncline basins, Journal of Structural Geology, 115, 208-230.
651 in press, doi: 10.1016/ j.jsg.2018.07.016.

652 Pichel, L. M., Huuse, M., Redfern, J., & Finch, E. (2019a). The influence of base-salt
653 relief, rift topography and regional events on salt tectonics offshore Morocco. Marine
654 and Petroleum Geology, 103, 87-113.

655 Pichel, L. M., Finch, E., & Gawthorpe, R. L. (2019b). The Impact of Pre-Salt Rift
656 Topography on Salt Tectonics: A Discrete-Element Modeling Approach. Tectonics,
657 38(4), 1466-1488.

658 Pichel, L. M., Jackson, C. A. L., Peel, F., & Dooley, T. P. (2019c). Base-salt relief
659 controls salt-tectonic structural style, São Paulo Plateau, Santos Basin, Brazil. Basin
660 Research.

661 Pichel, L. M., & Jackson, C. A-L., (2020) Four-dimensional Variability of Composite
662 Halokinetic Sequences. Basin Research.

663 Quirk, D. G., Schødt, N., Lassen, B., Ings, S. J., Hsu, D., Hirsch, K. K., Von Nicolai, C.
664 (2012). Salt tectonics on passive margins: examples from Santos, Campos and
665 Kwanza basins. Geological Society, London, Special Publications, 363(1), 207-244.

666 Quirk, D. G., & Pilcher, R. S. (2012). Flip-flop salt tectonics. Geological Society,
667 London, Special Publications, 363(1), 245-264.

668 Roberts, A. M., Kusznir, N. J., Yielding, G., & Styles, P. (1998). 2D flexural
669 backstripping of extensional basins; the need for a sideways glance. Petroleum
670 Geoscience, 4(4), 327-338.

671 Rodriguez, C. R., Jackson, C. L., Rotevatn, A., Bell, R. E., Francis, M. (2019). Dual
672 tectonic-climatic controls on salt giant deposition in the Santos Basin, offshore Brazil.
673 Geosphere, 14(1), 215-242.

674 Rowan, M. G., Lawton, T. F., Giles, K. A., & Ratliff, R. A. (2003). Near-salt deformation
675 in La Popa basin, Mexico, and the northern Gulf of Mexico: A general model for
676 passive diapirism. AAPG bulletin, 87(5), 733-756.

677 Rowan, M. G., Peel, F. J., & Vendeville, B. C. (2004). Gravity-driven fold-belts on
678 passive margins.

679 Rowan, M. G., & Ratliff, R. A. (2012). Cross-section restoration of salt-related
680 deformation: Best practices and potential pitfalls. Journal of Structural Geology, 41,
681 24-37.

682 Rowan, M. G., Giles, K. A., Hearon IV, T. E., Fiduk, J. C. (2016). Megaflaps adjacent
683 to salt diapirs. AAPG Bulletin, 100(11), 1723-1747.

684 Sclater, J. G., & Christie, P. A. (1980). Continental stretching: An explanation of the
685 post-mid-Cretaceous subsidence of the central North Sea basin. Journal of
686 Geophysical Research: Solid Earth, 85(B7), 3711-3739.

687 Scotchman, I. C., Marais-Gilchrist, G., Souza, F., Chaves, F. F., Atterton, L. A.,
688 Roberts, A., & Kusznir, N. J. (2006). A failed sea-floor spreading centre, Santos Basin,
689 Brasil. In Rio Oil & Gas Expo and Conference. Rio de Janeiro, Brazil, Brazilian
690 Petroleum, Gas and Biofuels Institute.

691 Scotchman, I. C., Gilchrist, G., Kusznir, N. J., Roberts, A. M., & Fletcher, R. (2010).
692 The breakup of the South Atlantic Ocean: formation of failed spreading axes and
693 blocks of thinned continental crust in the Santos Basin, Brazil and its consequences
694 for petroleum system development. In Geological Society, London, Petroleum
695 Geology Conference series (Vol. 7, No. 1, pp. 855-866). Geological Society of London.

696 Szatmari, P. M. C. M., Guerra, M. C. M., & Pequeno, M. A. (1996). Genesis of large
697 counter-regional normal fault by flow of Cretaceous salt in the South Atlantic Santos
698 Basin, Brazil. Geological Society, London, Special Publications, 100(1), 259-264.

699 Vendeville, B. C., Jackson, M. P. A. (1992). The rise of diapirs during thin-skinned
700 extension. Marine and Petroleum Geology, 9(4), 331-354.

FIGURES

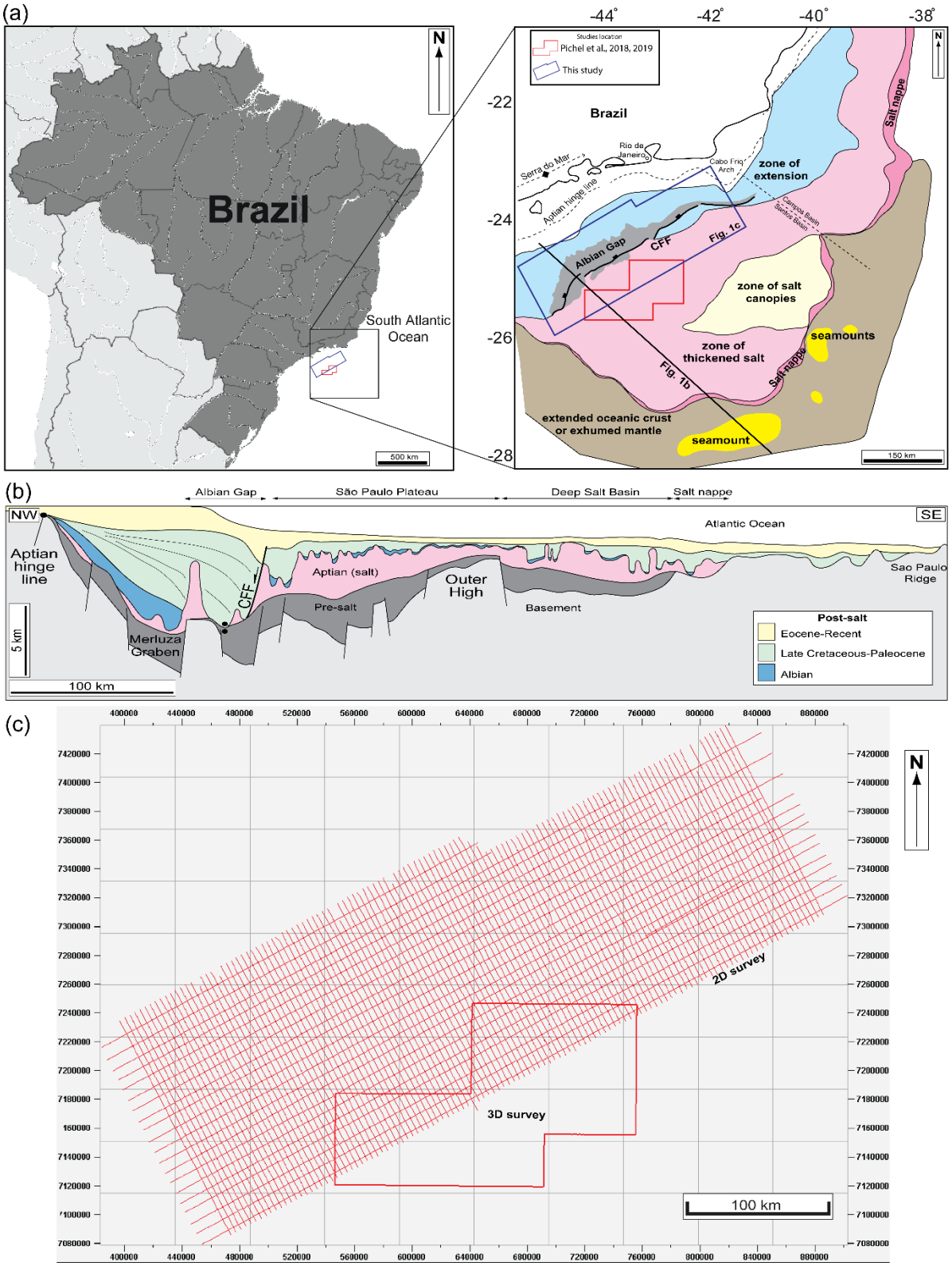

Fig. 1: (a) Map and (b) regional geoseismic cross-section showing the main regional salt-related structural domains offshore the Santos Basin and location of the study-area and

seismic survey used in the study (adapted from Davison et al., 2012). (c) 2D and 3D seismic survey used in the study.

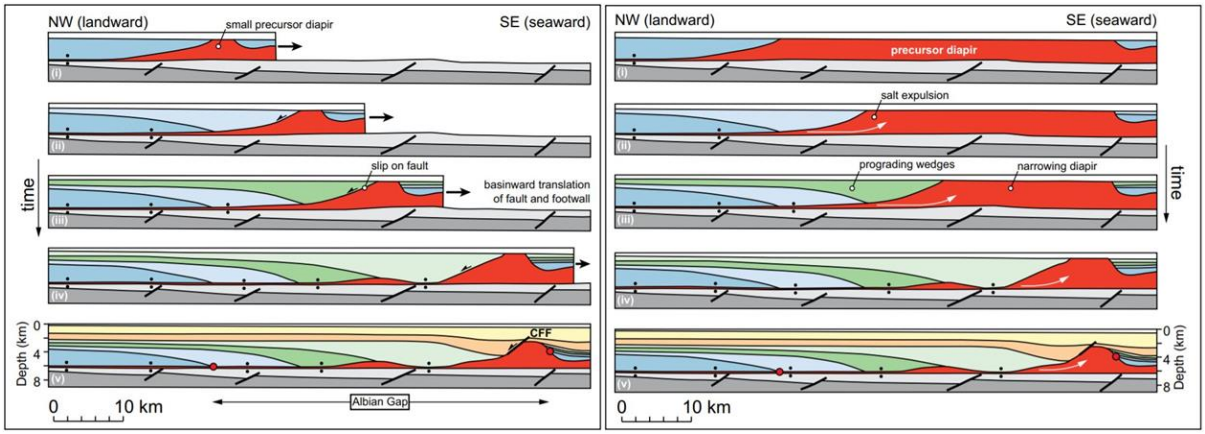

Fig. 2: Competing end-member models of the origin and evolution of the Albian Gap: (a) post-Albian extension; (b) post-Albian salt expulsion and basinward inflation (adapted from Rowan and Ratliff, 2012, no vertical exaggeration). Note flat datum during each restoration step.

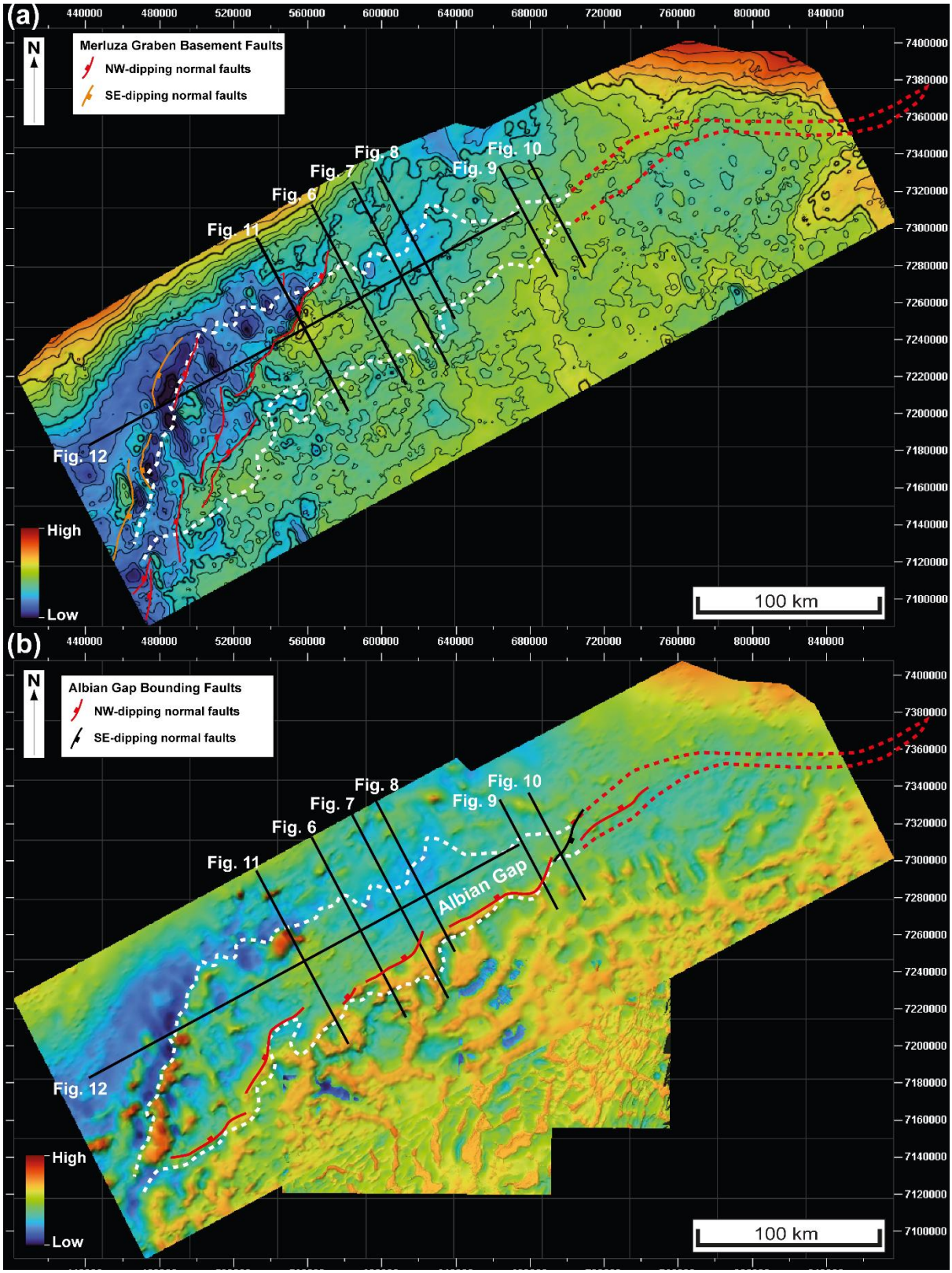

Fig. 3: (a) Base-salt map showing the location of main pre-salt rift faults associated with the Merluza Graben. (b) Top-Salt map showing the distribution of main salt-detached thin-skinned normal faults within the Albian Gap. Outline of the Albian Gap in dashed lines and seismic sections presented in the study in black.

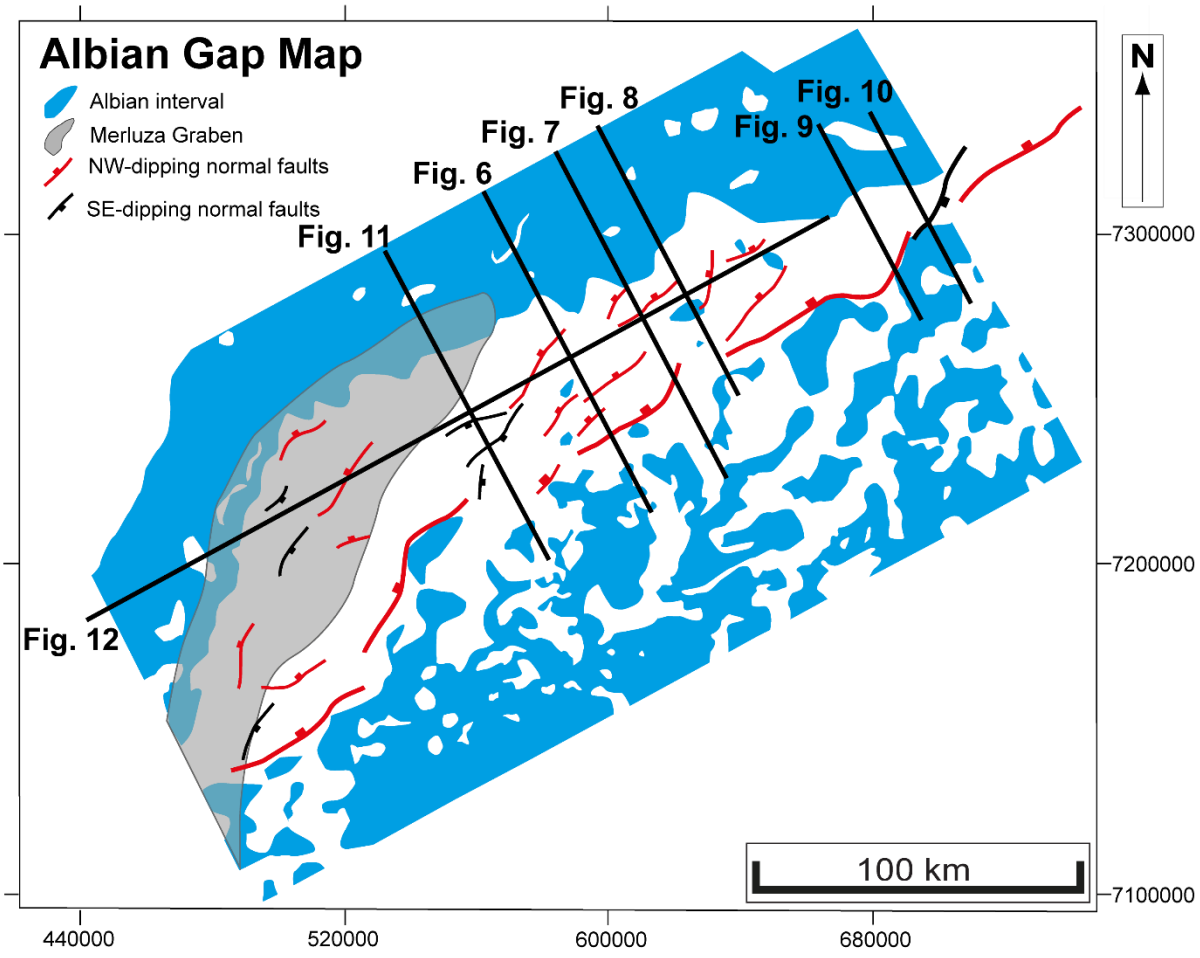

716

717 Figure 4: Map showing the distribution of the Albian interval and outline of the Albian Gap in

718 the study-area. The pre-salt Merluza Graben and the main salt-detached normal faults

719 associated with the Albian Gap rollover are also indicated.

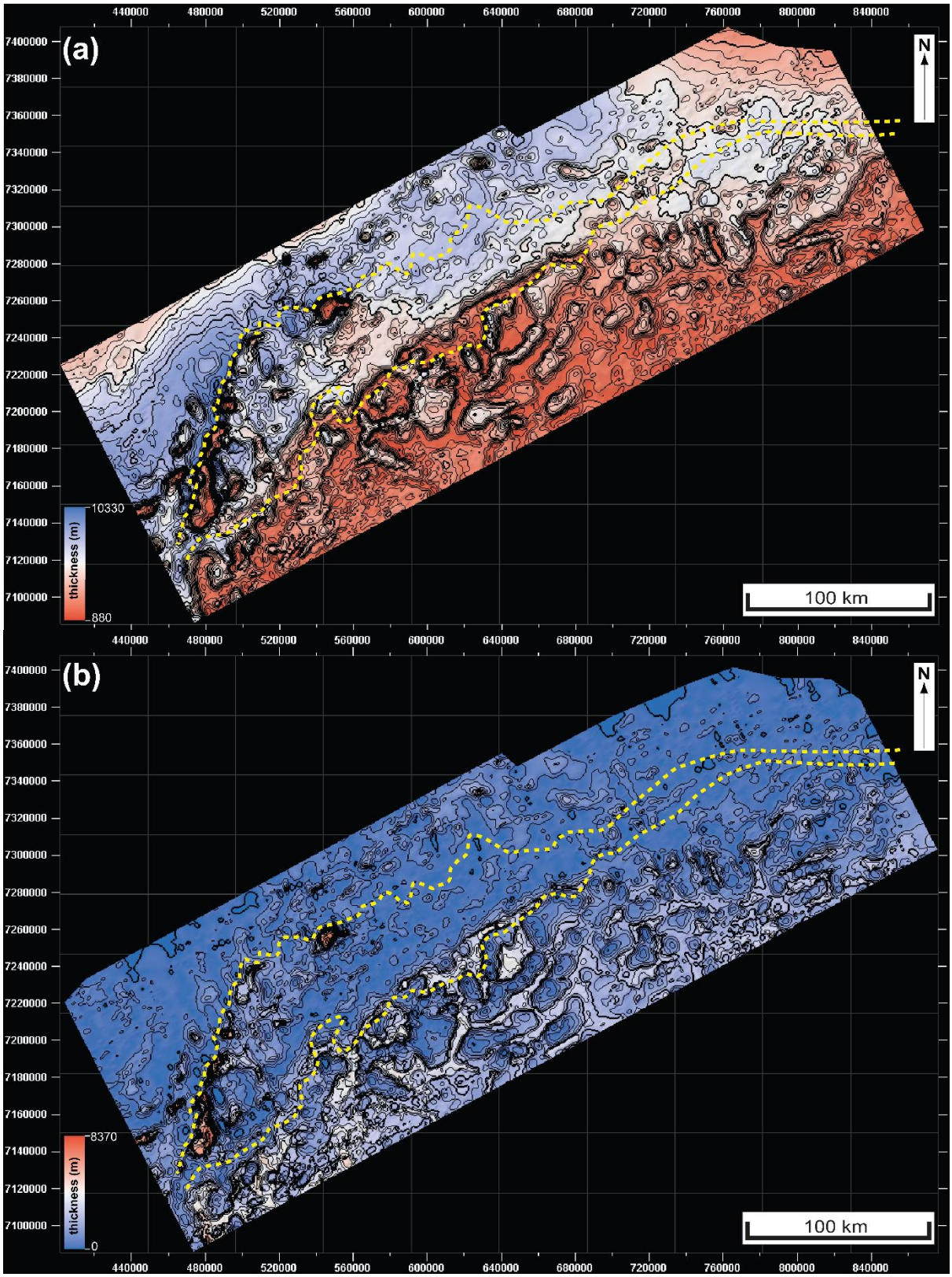

Fig. 5: (a) Overburden thickness map and (b) salt thickness map. The maximum overburden thickness (9-10 km) and thinner (>200m) salt occur in the proximal domain within the Albian Gap. Albian Gap outline in yellow dashed line.

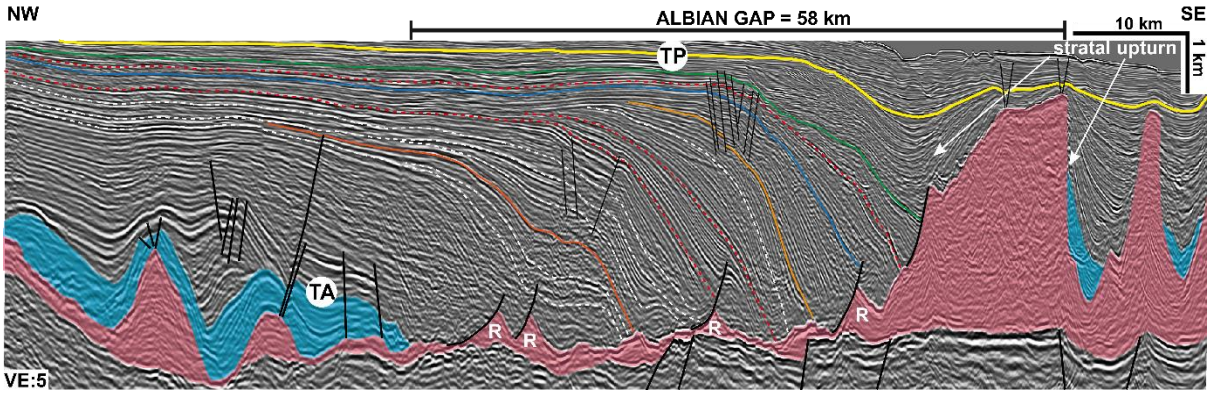

Figure 6: South-central dip-oriented section from the Albian Gap. Salt in pink, Albian in blue and normal faults in black. An intra-Paleogene regional unconformity in yellow. The gap is 58 km wide being composed by a 50 km wide basinward-dipping rollover and an 8 km wide salt wall with strata upturn on both its flanks. The post-Albian rollover presents contrasting growth wedges: basinward-thinning sigmoidal wedges (white) and basinward-thickening wedges (red). The gap is also associated with small landward-dipping listric normal faults that become progressively younger basinward. For correlation purposes, key stratigraphic horizons are indicated in orange, yellow, blue and green; see the following figures. Small salt rollers indicated by (R). Seismic data courtesy of TGS and WesternGeco.

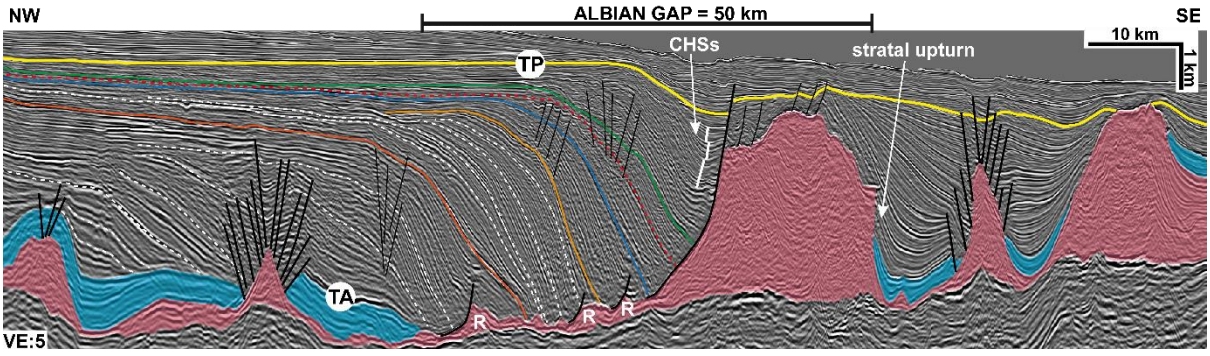

Figure 7: Central dip-oriented section from the Albian Gap. Salt in pink, Albian in blue and normal faults in black. An intra-Paleogene regional unconformity in yellow. The gap is 50 km wide being composed of a 40 km wide basinward-dipping rollover and a 10 km wide salt wall with strata upturn and halokinetic sequences (thick white lines) on its flanks and a large landward-dipping normal fault on its landward side. The post-Albian rollover presents

contrasting growth wedges: basinward-thinning sigmoidal wedges (white) and basinward-thickening wedges (red). The gap is also associated with small landward-dipping listric normal faults that become progressively younger basinward. For correlation purposes, key stratigraphic horizons are indicated in orange, yellow, blue and green; see following figures. Small salt rollers indicated by (R). Seismic data courtesy of TGS and WesternGeco.

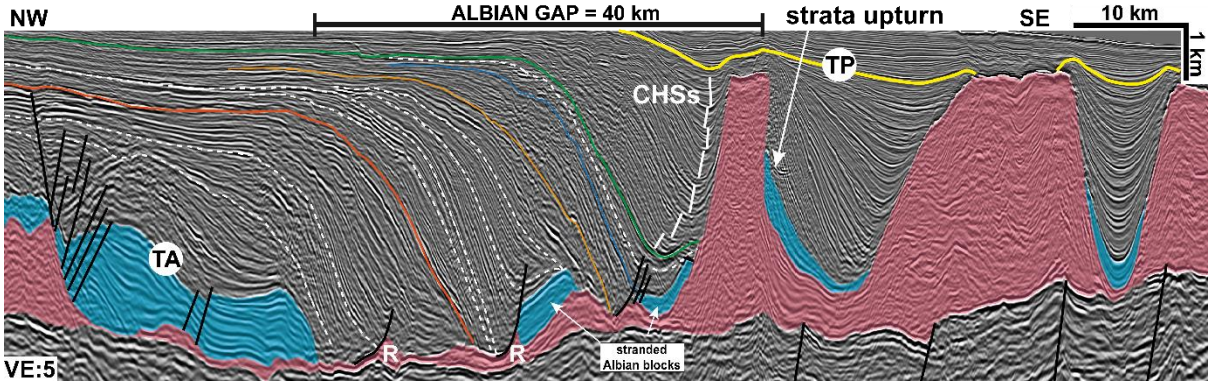

Figure 8: Central-north dip-oriented section from the Albian Gap. Salt in pink, Albian in blue and normal faults in black. An intra-Paleogene regional unconformity in yellow. The gap is 40 km wide being composed of a 37 km wide basinward-dipping rollover and 3 km wide salt wall with strata upturn and halokinetic sequences (thick white lines) on its flanks. The post-Albian rollover presents contrasting growth wedges: basinward-thinning sigmoidal wedges (white) and basinward-thickening wedges (red). The gap is also associated with small landward-dipping listric normal faults that become progressively younger basinward and occasionally downlap remnant Albian blocks. For correlation purposes, key stratigraphic horizons are indicated in orange, yellow, blue and green; see the following figures. Small salt rollers indicated by (R). Seismic data courtesy of TGS and WesternGeco.

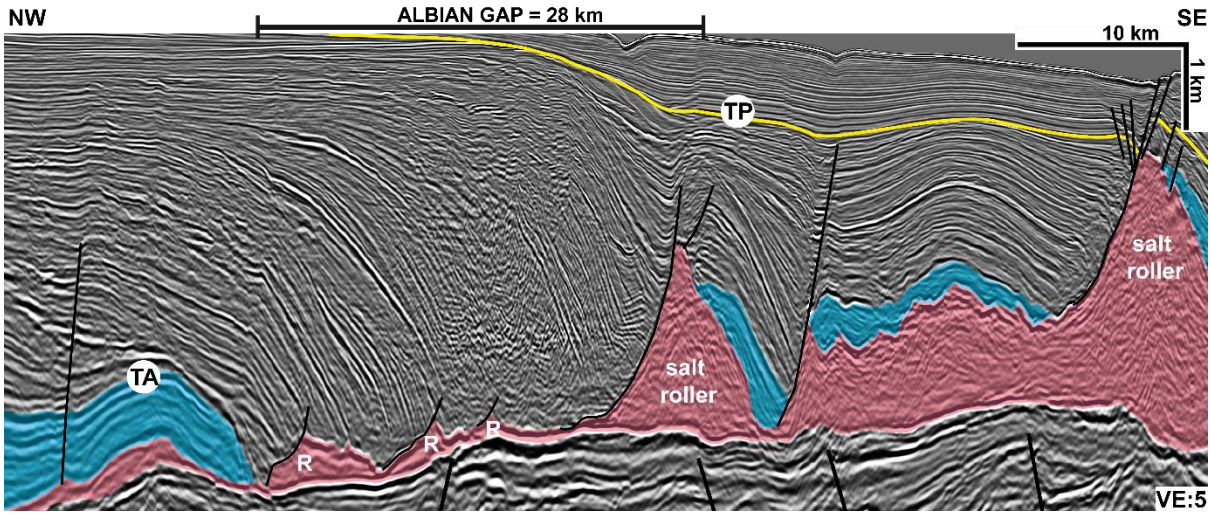

Figure 9: North dip-oriented section from the Albian Gap. Salt in pink, Albian in blue and normal faults in black. An intra-Paleogene regional unconformity in yellow. The gap is 28 km wide being composed of a 27 km wide basinward-dipping rollover and c.1 km wide reactive (extensional) salt wall/roller defined by a large landward-dipping normal fault. The post-Albian rollover presents dominant basinward-thickening wedges associated with small landward-dipping listric normal faults that become progressively younger basinward. Small salt rollers indicated by (R). Seismic data courtesy of TGS and WesternGeco.

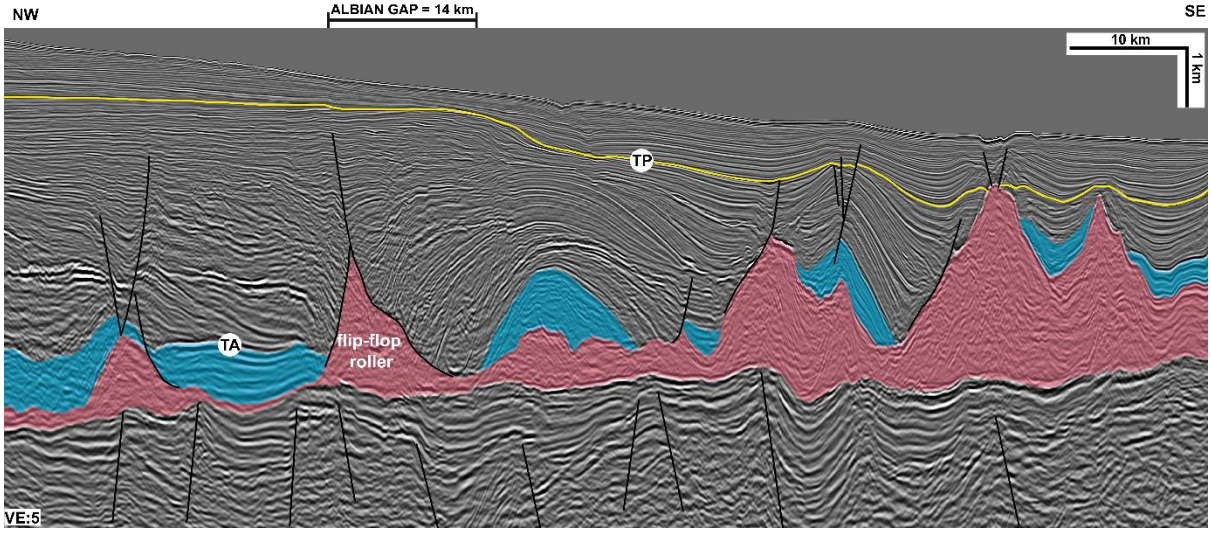

Figure 10: Northernmost section illustrating the switch in fault polarity associated with a flip-flop salt reactive diapir bounding the Albian Gap. The gap is significantly narrower (14 km) and associated with a wide 35 km wide extensional turtle anticline further downdip. Seismic data courtesy of TGS and WesternGeco.

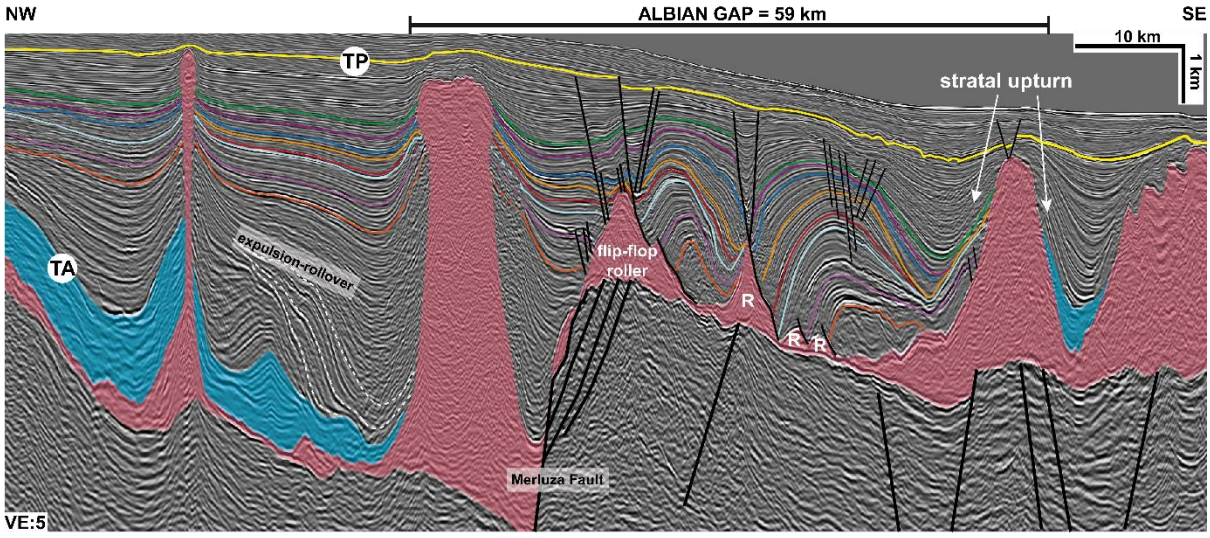

Figure 11: Central dip-oriented section from the Albian Gap. Salt in pink, Albian in blue and normal faults in black. An intra-Paleogene regional unconformity in yellow. The gap is 58 km wide. It comprises the downdip edge of the Merluza Graben and the related 8 km, 8.5 km tall salt stock at its hangingwall. Further downdip the Albian Gap is defined by two large salt rollers, the updip one with a flip-flop geometry and basinward-dipping listric normal faults predominate. The gap is bounded downdip by a diapir that shows significant strata upturn on its both flanks. Key stratigraphic horizons are indicated coloured for correlation purposes, see previous sections. Small salt rollers indicated by (R). Seismic data courtesy of TGS and WesternGeco.

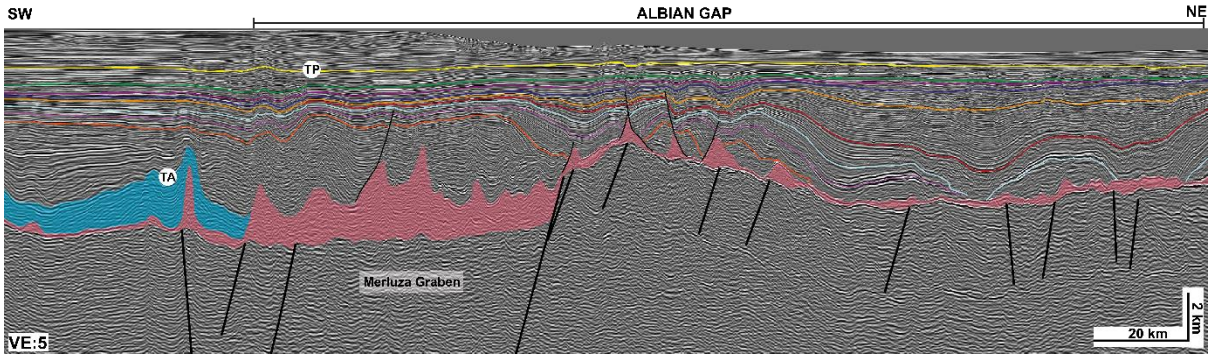

Figure 12: Strike-section illustrating the thickness variations with the Albian Gap and its relationship with the Merluza Graben to the south. Salt in pink, Albian in blue and normal faults in black. An intra-Paleogene regional unconformity in yellow. The overburden is 9-10 km to

the south, with the post-Albian rollover being up to 9 km thick; whereas to the north it is on average 6-7 km thick. Seismic data courtesy of TGS and WesternGeco.

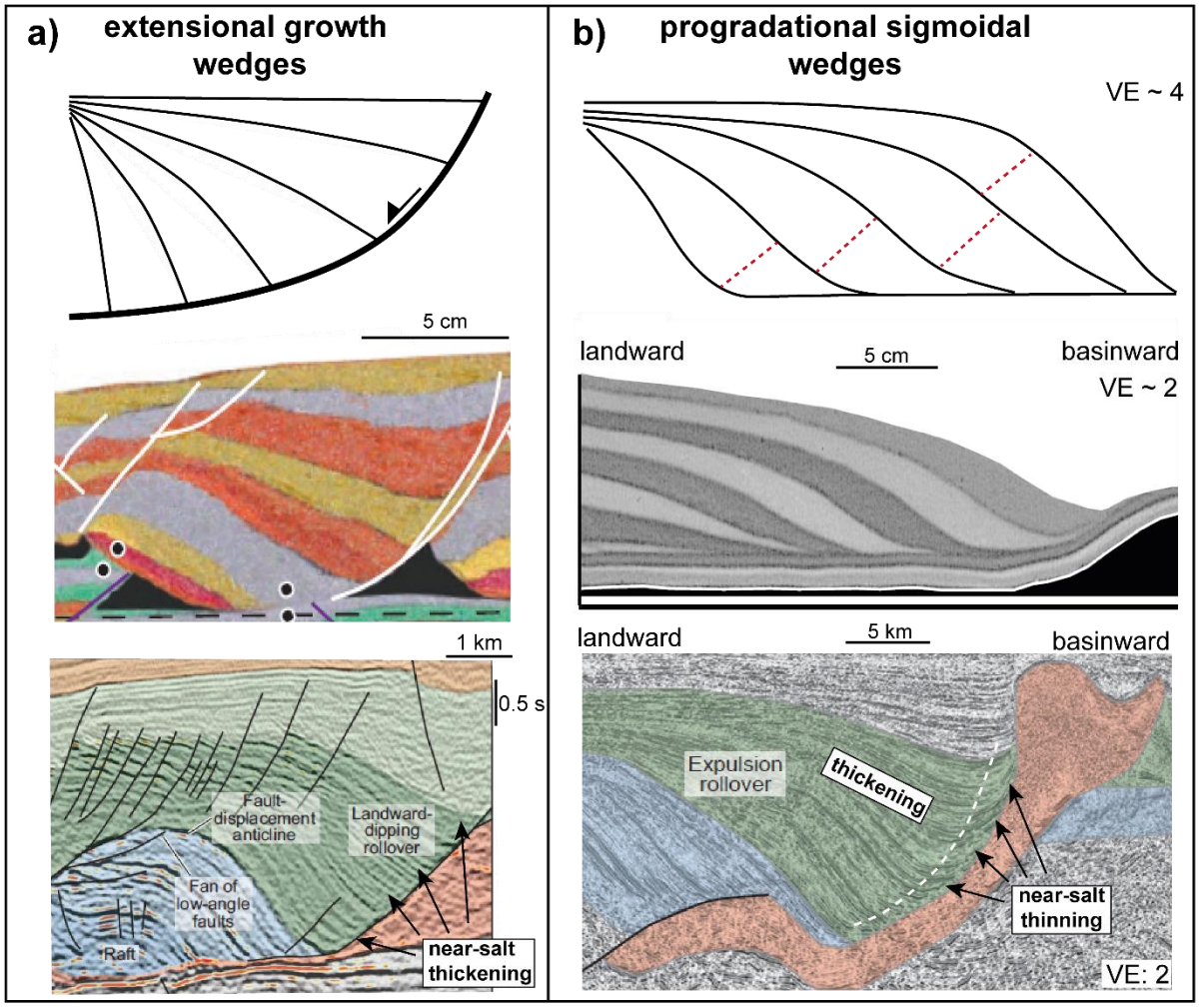

Figure 13: Different styles of rollover growth wedges: a) basinward-thickening extensional wedges with a physical model example in the second row (adapted from Jackson and Hudec, 2017) and a seismic example from the Kwanza Basin, Angola in the third-row (after Chimney and Kluk, 2002 and Jackson and Hudec, 2017), and b) basinward-thinning clinoform sigmoidal growth wedges with a physical model example in the second row (adapted from Ge et al., 1997) and a seismic example from the Gulf of Mexico (adapted from Jackson and Hudec, 2017).

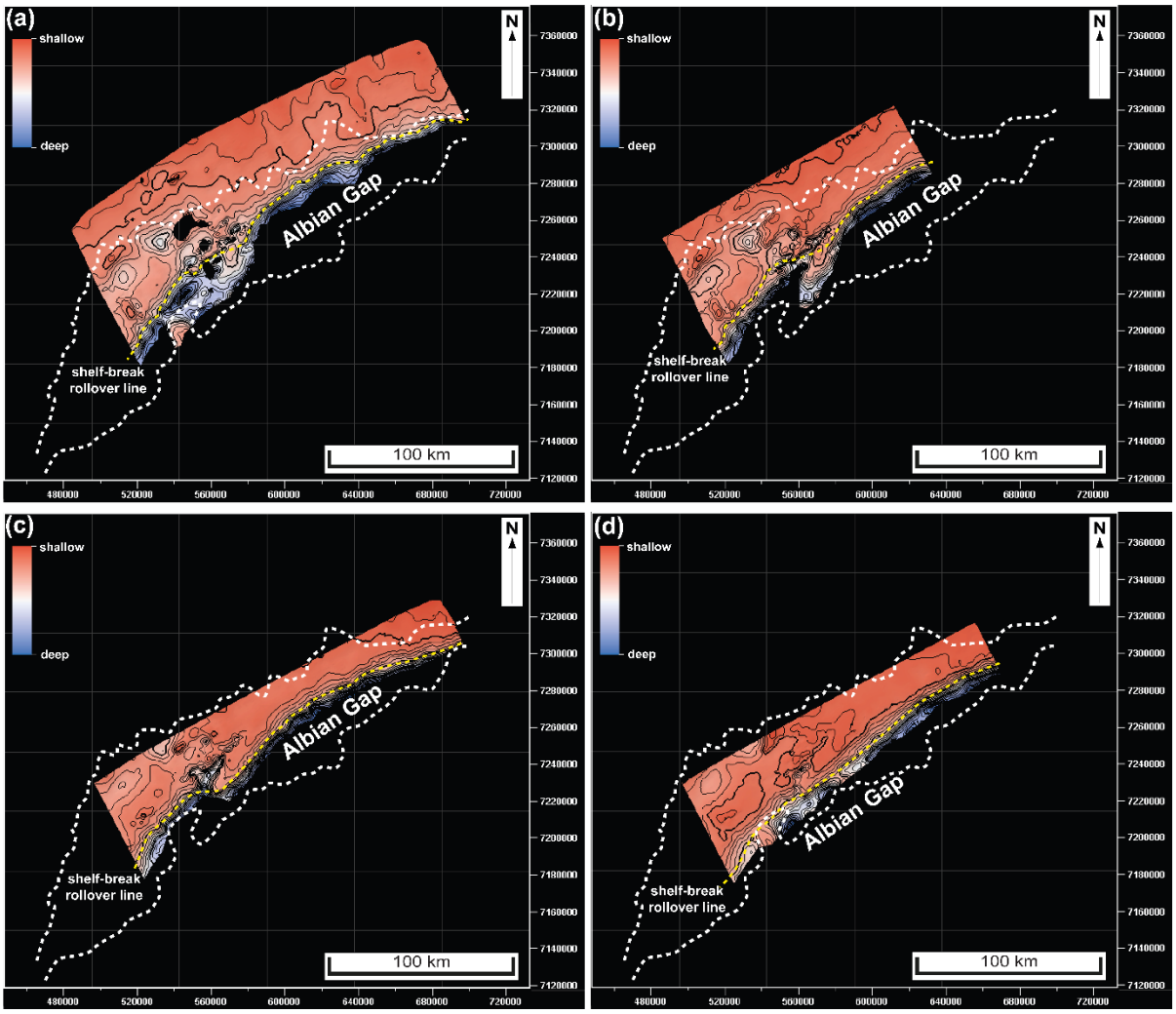

Figure 14: Structural maps of key stratigraphic intervals within the post-Albian rollover in the Albian Gap: (a) orange, (b) yellow, (c) blue and (d) green from cross-sections (figs. 6-8). The maps demonstrate that in the central-south portion where the Albian gap is wider, the shelf-break rollover point was located further basinward, indicating greater progradation of sediments.

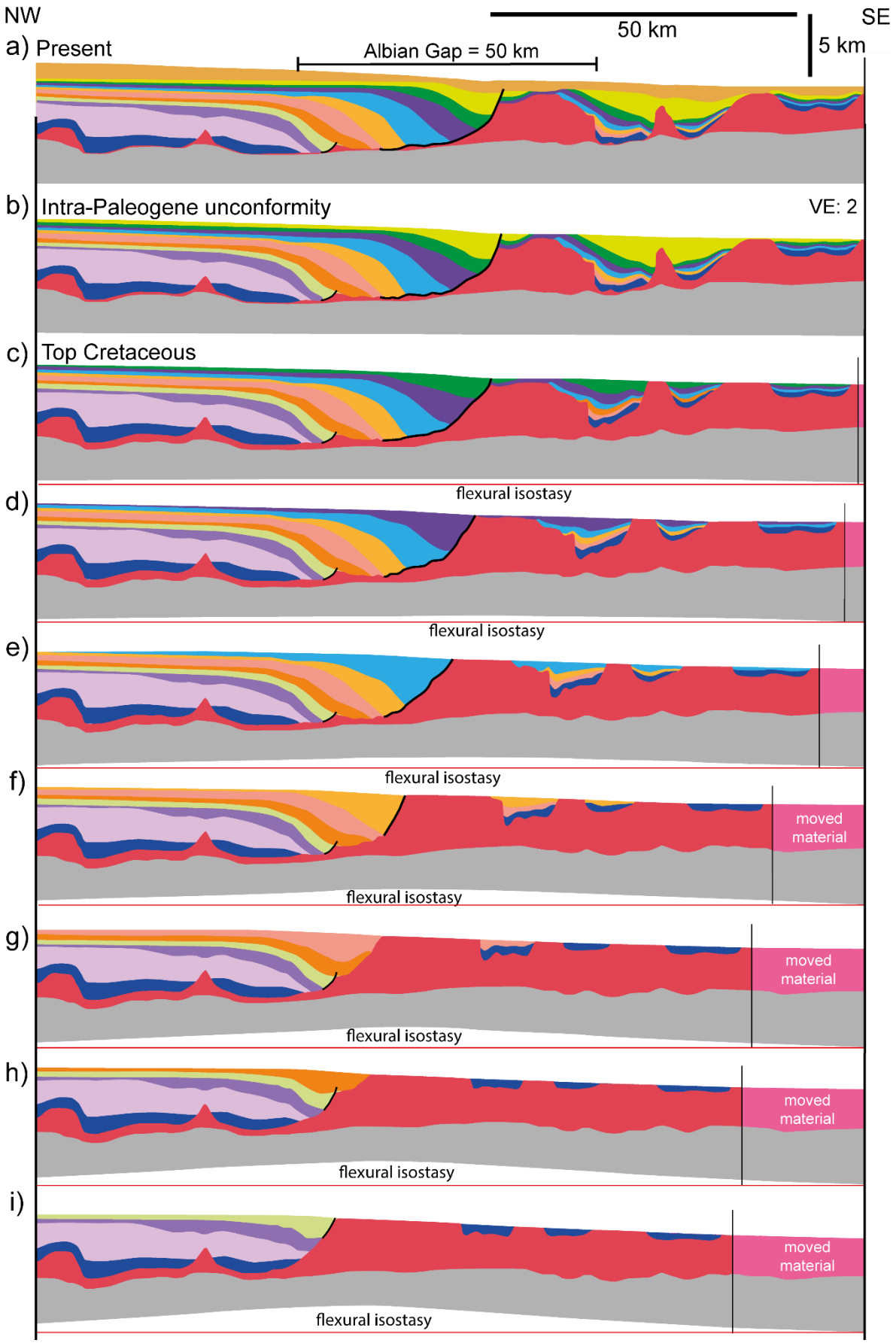
NW
SE
50 km
5 km
a) Present
Albian Gap = 50 km
b) Intra-Paleogene unconformity
VE: 2
c) Top Cretaceous
d)
flexural isostasy
e)
flexural isostasy
f)
flexural isostasy
moved material
flexural isostasy
g)
moved material
flexural isostasy
h)
moved material
flexural isostasy
i)
moved material
flexural isostasy

802

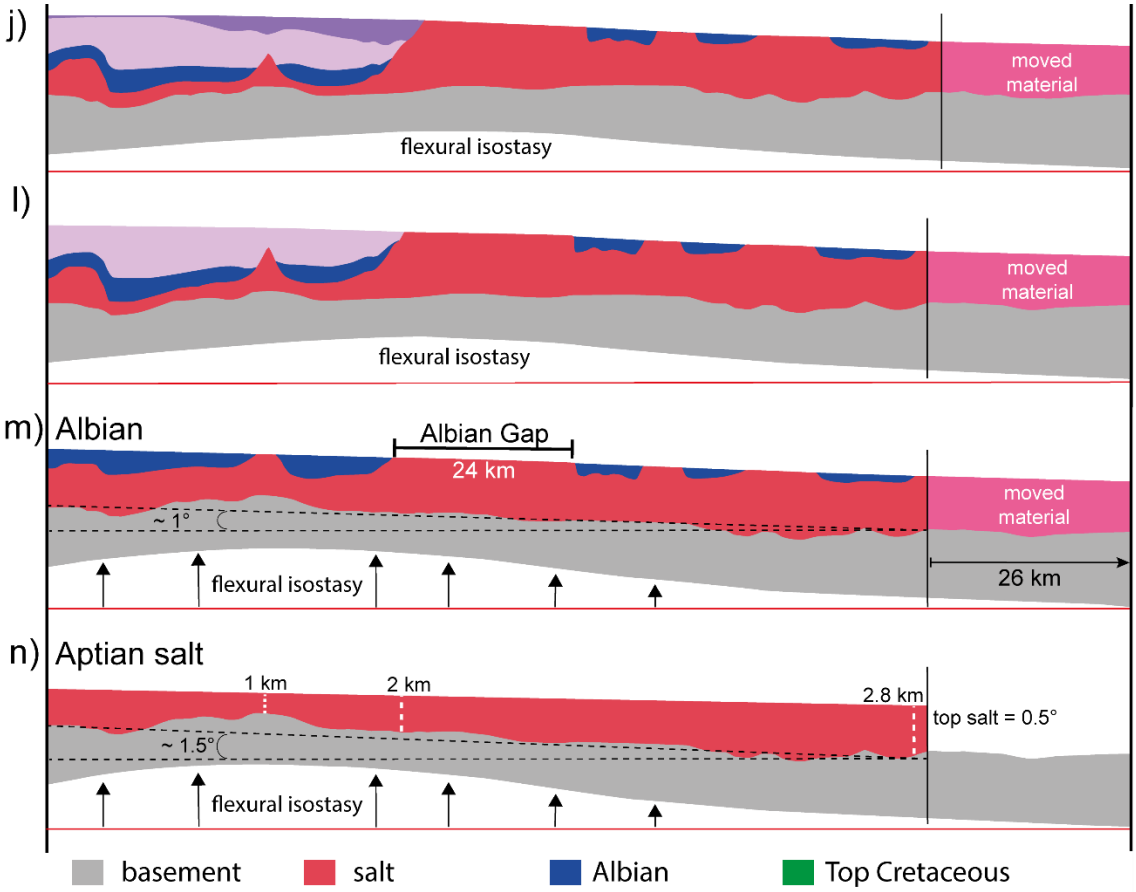

Figure 15: Detailed sequential restoration of the central and most representative section from the Albian Gap involving decompaction, unfolding, move on fault and flexural isostasy. (a) The Albian Gap is at present 50 km wide. Decompaction and unfolding of post-Albian sequences (b-l) demonstrates that during that time, the Albian Gap accommodated 26 km of extension and that the Albian Gap was partially formed as a 24 km (± 2) wide passive salt wall during the Albian. During the Aptian (n) and Albian (m), the base-salt dipped regionally > 1º basinward but flipped gradually through time during the deposition of the anomalously thick post-Albian rollover within the Albian Gap.

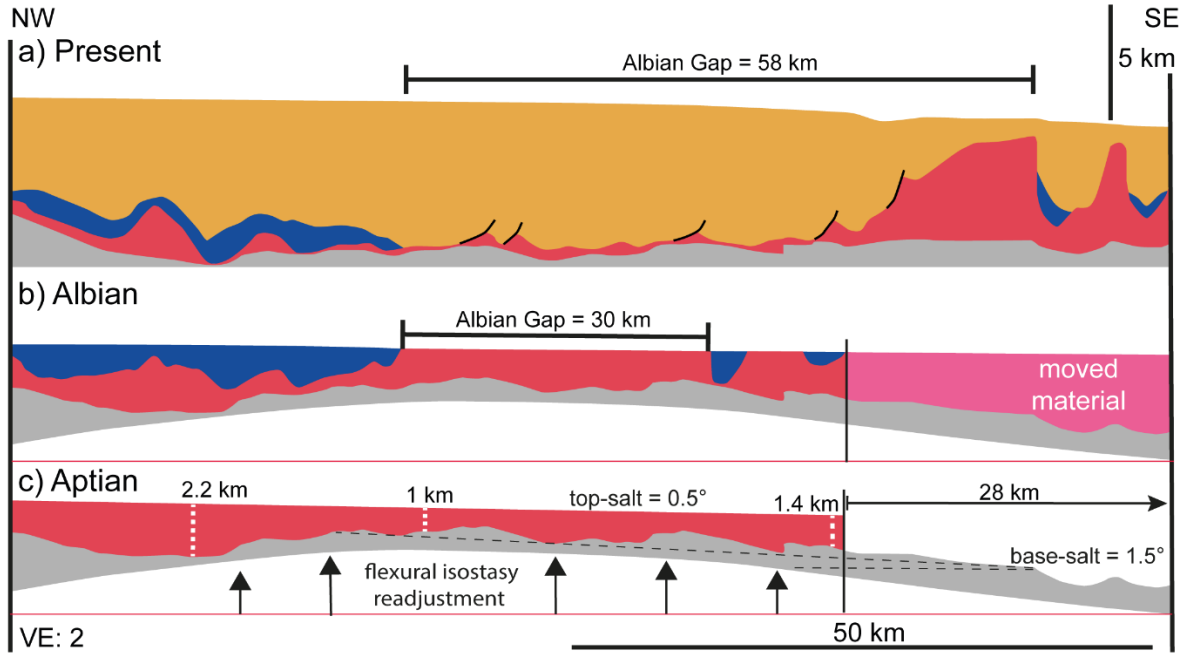

Figure 16: Restoration of a section over the southern portion of the Albian Gap (Fig. 6) showing dip reversal of the base-salt by flexural isostasy due to the deposition of a c. 6-7 km thick post-Abian rollover (fig. 9). The Albian Gap is at present 58 km, resulting from a combination from post-Albian extension (28 km) and salt expulsion from a 30 km wide Albian salt wall.

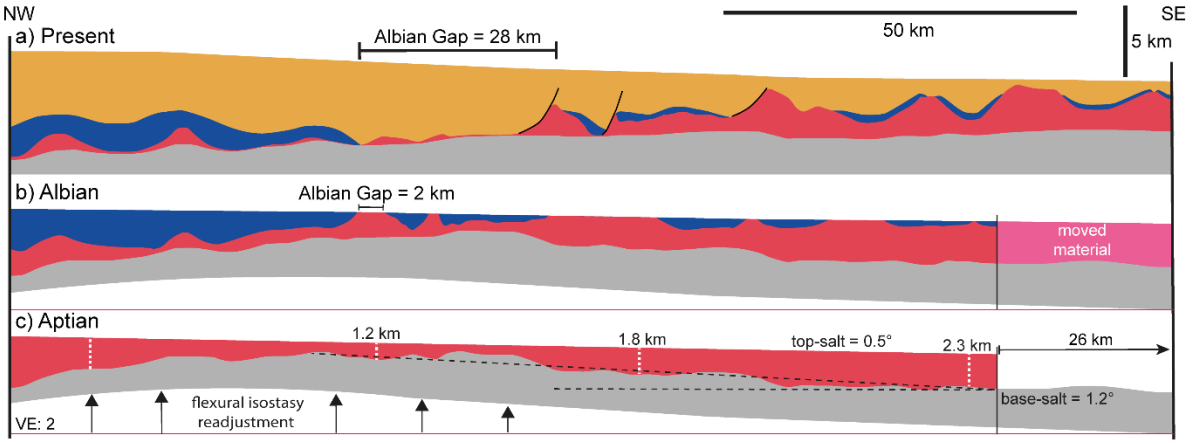

Figure 17: Restoration of section over the northern portion of the Albian Gap showing dip reversal of the base-salt by flexural isostasy due to the deposition of a c. 5 km thick post-Albian rollover (fig. 9). The Albian Gap is at present 28 km, resulting primarily of post-Albian extension (26 km).

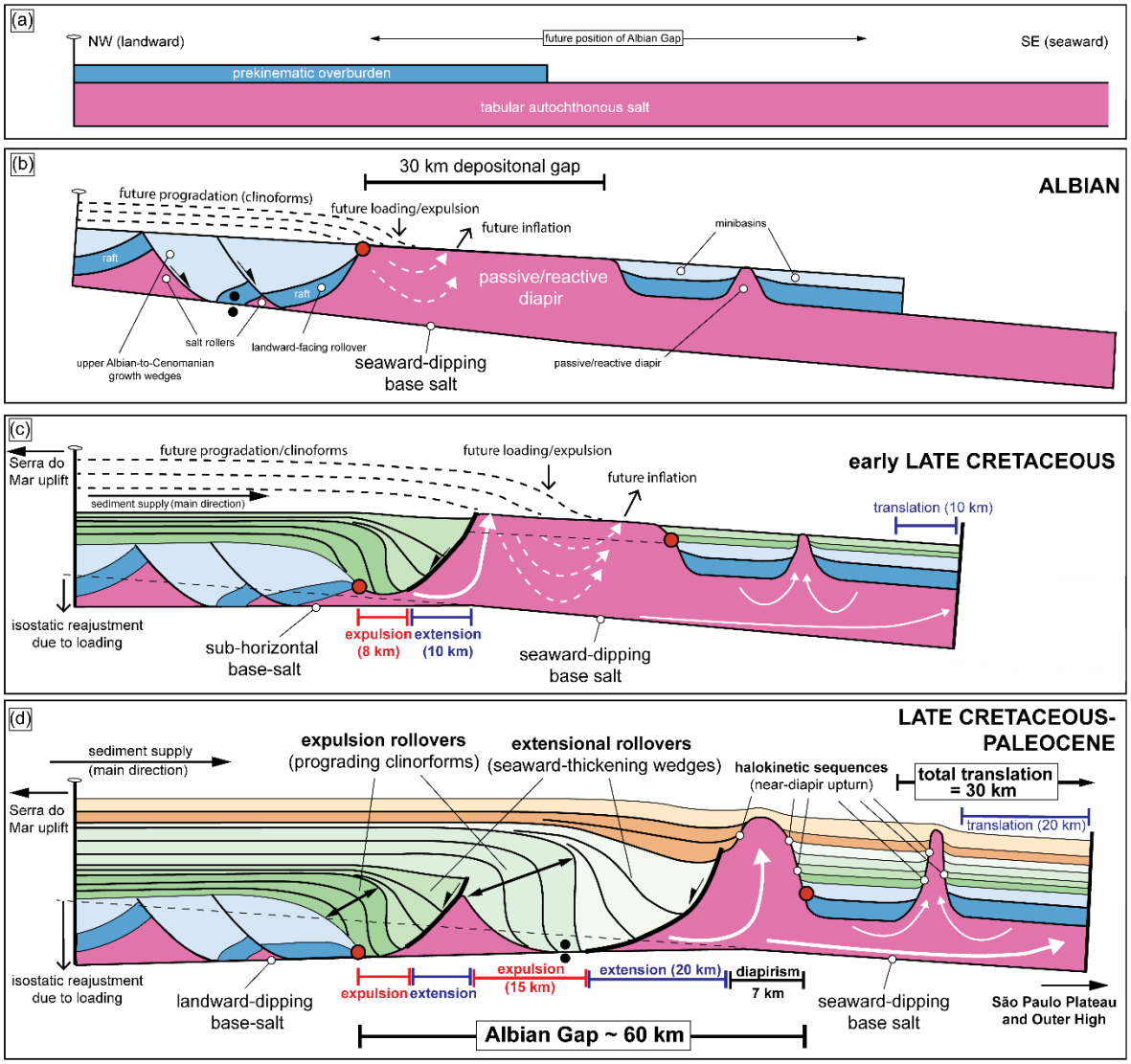

Figure 18: New kinematic model explaining the origin and evolution of the Albian Gap. (a-b) During the Albian, salt deformation was controlled by salt detached extension with basinward-dipping normal faults and development of a 30 km wide reactive/passive diapir downdip. (c) During the early Late Cretaceous, margin-scale progradation of sediments over the earlier-formed passive salt wall resulted in develop of small landward-dipping normal faults (extension) and salt expulsion (differential loading) from the diapir onto the São Paulo Plateau further downdip. (d) Continuous progradation resulted in further extension with development of larger landward-dipping faults due to progressive landward-rotation of the base-salt caused by isostatic readjustment of the base-salt, and salt expulsion within the Albian Gap, salt inflation, active diapirism and translation further downdip.